Research Paper

GEOSPHERE

GEOSPHERE; v. 13, no. 3

doi:10.1130/GES01457.1

21 figures; 3 supplemental files

CORRESPONDENCE: paulfhoffman@gmail.com

CITATION: Hoffman, P.F., Lamothe, K.G., LoBianco, S.J.C., Hodgskiss, M.S.W., Bellefroid, E.J., Johnson, B.W., Hodgin, E.B., and Halverson, G.P., 2017, Sedimentary depocenters on Snowball Earth: Case studies from the Sturtian Chuos Formation in northern Namibia: Geosphere, v. 13, no. 3, p. 811–837, doi:10.1130/GES01457.1.

Received 5 November 2016
Revision received 14 January 2017
Accepted 1 March 2017
Published online 7 April 2017

Sedimentary depocenters on Snowball Earth: Case studies from the Sturtian Chuos Formation in northern Namibia

Paul F. Hoffman[1,2], Kelsey G. Lamothe[3], Samuel J.C. LoBianco[1], Malcolm S.W. Hodgskiss[3,4], Eric J. Bellefroid[5], Benjamin W. Johnson[2], E. Blake Hodgin[1], and Galen P. Halverson[3]

[1]Department of Earth and Planetary Sciences, Harvard University, Cambridge, Massachusetts 02138, USA
[2]School of Earth and Ocean Sciences, University of Victoria, Victoria, British Columbia V8P 5C2, Canada
[3]Department of Earth and Planetary Sciences, McGill University, Montreal, Quebec H3A 0E8, Canada
[4]Department of Geological Sciences, Stanford University, Stanford, California 94305, USA
[5]Department of Geology and Geophysics, Yale University, New Haven, Connecticut 06520-8109, USA

ABSTRACT

Cryogenian synglacial deposits are regionally thin but locally thick, considering glacial duration, but the reasons for local thickening are poorly known. We studied three local thickenings of the Sturtian Chuos Formation in northern Namibia by measuring closely spaced columnar sections, not only of the synglacial deposits but also of the bounding pre- and post-glacial strata. This enabled incised paleovalleys filled by glacial debris to be distinguished from morainal buildups. In case 1, a U-shaped paleovalley, ~450 m deep by ~3.0 km wide, is incised into pre-glacial strata and 10% overfilled by ice-contact and subglacial meltwater deposits. In case 2, a wedge of glacial diamictite, ~220 m thick by 2.0 km wide, overlies a disconformity that is demonstrably not incised into underlying pre-glacial strata. The wedge, draped by a post-glacial cap carbonate and argillaceous strata, is erosionally truncated at its apex by Marinoan glacial deposits and their basal Ediacaran cap dolomite. The wedge was a positive topographic feature, either a terminal moraine or an erosional outlier of formerly more extensive glacial deposits. In case 3, a wedge of conglomerate, glacial diamictite, and subglacial lake deposits thickens to >2000 m where it abuts against granitoid basement rock uplifted along a border fault. Fault movement ceased before the Sturtian cap carbonate was deposited. The locus of maximum deposition shifted over time from proximal to distal with respect to the border fault, similar to Mesozoic half grabens developed above listric detachments imaged seismically on offshore North Atlantic margins.

INTRODUCTION

Globally, Cryogenian glacial deposits accumulated three to ten times slower than their Phanerozoic counterparts, averaged over comparable durations (Partin and Sadler, 2016). This holds in spite of the fact that Cryogenian glacial deposits formed at significantly lower paleomagnetic latitudes (Evans, 2003; Evans and Raub, 2011). These observations are consistent with the weak hydrologic cycle of a Snowball Earth (Abbot et al., 2013; Partin and Sadler, 2016).

Statistically, Cryogenian glacial deposits are regionally thin, with median thicknesses of ~50 m and ~25 m for the entire Sturtian (58 m.y.) and Marinoan (5–15 m.y.) cryochrons (Snowball Earth episode, Hoffman et al., 1998a), respectively (Rooney et al., 2015; Partin and Sadler, 2016). Yet, they attain thicknesses of hundreds to thousands of meters locally. What accounts for local overthickened glacial deposits on a postulated Snowball Earth?

We investigated three localized depocenters (cases 1–3 hereafter) in the Chuos Formation, which represents the Sturtian cryochron in central and northern Namibia (Hoffmann and Prave, 1996; Miller, 2008). The stratigraphic base and top of this formation are clearly defined in these areas, as is characteristic of Cryogenian glacigenic formations generally. The median thickness of all the complete Chuos Formation sections we have measured (n = 88) is 48.2 m (Fig. 1). In the three depocenters described herein, the Chuos Formation reaches roughly 4.5, 10, and 40 times its median thickness.

Our first task was to identify those depocenters associated with incised paleovalleys. To this end, we measured closely spaced (<1.0 km) columnar sections of the sub-Chuos (pre-glacial) formations of the late Tonian Ugab and Ombombo Subgroups (Fig. 2). Their stratigraphy was known on a regional scale from previous work (Miller, 1980; Clifford, 2008; Hoffman and Halverson, 2008). In case 1 (Omutirapo springs), we found that Chuos thickening is quantitatively

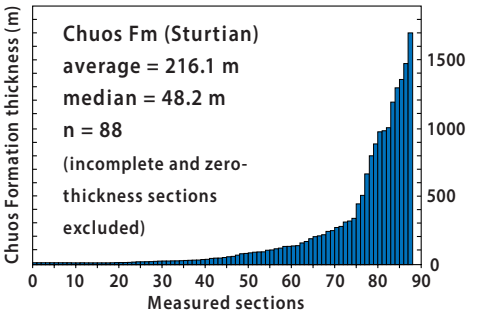

Figure 1. Bar graph of syn-glacial Chuos Formation stratigraphic thicknesses in 88 columnar sections (including 38 from this study) measured by the authors in northern Namibia, in order of increasing thickness from left to right.

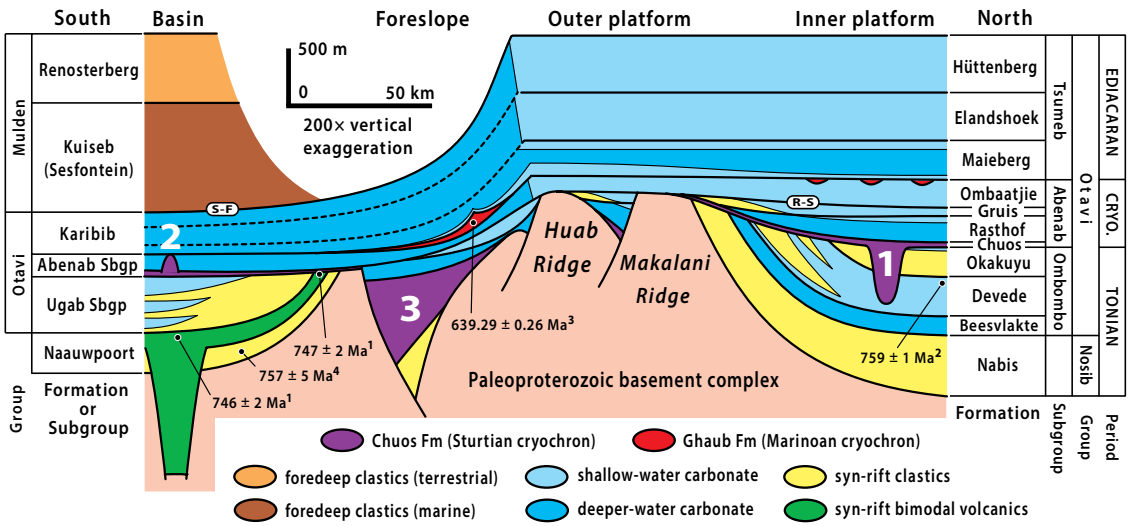

Figure 2. Schematic stratigraphic relations among Neoproterozoic strata in a north-south section across the southern Kunene Region, Namibia, from roughly 18°25′S, 13°45′E to 20°45′S, 14°45′E. Three case studies in the Chuos Formation are numbered 1–3. Horizon R-S (base of Ombaatjie Formation) is the rift-to-shelf transition, and horizon S-F (base of Kuiseb Formation) is the shelf–to–collisional foredeep transition (Hoffman and Halverson, 2008). Sources of U-Pb zircon dates: [1]Hoffman et al. (1996); [2]Halverson et al. (2005); [3]Prave et al. (2016); [4]Nascimento et al. (2016). Huab and Makalani Ridges are rift-shoulder uplifts associated with normal faults that are antithetic to the normal-sense detachment fault on Toekoms farm (case 3). Cryo.—Cryogenian.

accommodated by incision of the subglacial Ombombo Subgroup. The bedrock trough is symmetrical, ~450 m deep, and U-shaped with steep walls against which the synglacial valley-fill deposits abut. The trough is associated with a high-angle growth fault in the subglacial sequence, but the fault was demonstrably inactive during the Sturtian glaciation. The sedimentary fill compares with that of Quaternary subglacial bedrock troughs with transient meltwater cavities.

In case 2 (Vrede domes), measured sections imply no incision of the underlying Ugab Subgroup. Instead, a steep-sided wedge of Chuos diamictite with ~220 m of positive relief was draped and onlapped by basinal strata of the post-Sturtian nonglacial interlude. The Sturtian wedge was erosively decapitated during the subsequent Marinoan glaciation, with the result that the diamictite wedge and its draping Sturtian cap carbonate are truncated at their apex by a thin Marinoan diamictite and its distinctive basal Ediacaran cap dolomite.

Pre-Sturtian cover is absent in case 3 (Toekoms farm), where the Chuos Formation directly overlies crystalline basement rocks of Orosirian age. A 2-km-deep half graben is filled by synglacial rocks, whose facies distribution and geometry resemble those of syn-kinematic growth strata. Coarse-grained deposits—conglomerate, diamictite, and sandstone—thicken against a north-facing border fault. Distally, fine-grained subaqueous suspension deposits with turbidites, slumps, and occasional ice-rafted lonestones raise the possibility that the half graben developed into a subglacial lake or fjord. Up to 635 m of boulder conglomerate in the deepest part of the half graben lack glacial features and may be pre-Sturtian in age (McGee et al., 2012).

We begin by outlining the regional stratigraphy and structure, with emphasis on the Chuos Formation and the stratigraphically underlying and overlying subgroups (Fig. 2). Next we explain the descriptive terminology and classification scheme for our measured sections. Then we present each of our case studies in turn, as portrayed on cross-sections constructed from closely spaced columnar sections. Finally, we compare our findings with localized depocenters of glacial Cryogenian age in other regions, including Marinoan depocenters in northern Namibia formed when crustal stretching was no longer occurring on the Otavi platform.

REGIONAL STRATIGRAPHY

Although first named and interpreted as glacigenic in central Namibia (Gevers, 1931), the Chuos Formation is widely distributed in northern Namibia (Martin, 1965; Frets, 1969; Kröner and Rankama, 1972; Hedberg, 1979; Miller, 1980, 1997, 2008; Martin et al., 1985; Henry et al., 1986; Hoffmann and Prave, 1996; Clifford, 2008; McGee et al., 2012; Le Heron et al., 2013a, 2013b; Hoffman et al., 2016a; Nascimento et al., 2016). However, Sturtian and Marinoan syn-glacial deposits (Fig. 2) were not properly distinguished until after Hoffmann and Prave (1996).

The Chuos Formation is 0–2000 m thick (Fig. 1), and the predominant lithology in most sections is diamictite, wherein subrounded pebbles and boulders are suspended in an unsorted wackestone (micro-diamictite) matrix. The clasts and matrix are derived from the crystalline basement and from dolomite, quartz-arenite, and volcanic cover rocks. The relative proportions of basement- and cover-rock detritus are highly variable, but clast and matrix compositions commonly, but not invariably, covary. Faceted and striated clasts can be seen where tectonic strain is low (e.g., Le Heron et al., 2013a). Locally, diamictite is subordinate to co-derived clast-supported conglomerate and pebbly sandstone, or laminated argillite and siltstone with turbidites and ice-rafted debris. The Chuos Formation is distinctly enriched in ferric Fe (Martin, 1964;

SUPPLEMENTAL INFORMATION

Table S1 - Coordinates of measured columnar sections

Sections are keyed to figures and ordered from left to right across the figure.

Section #	Base (latitude, longitude, in °)	Top (latitude, longitude, in °)
Figure 7. Omutirapo springs		
K1611	-19.147393, 13.933306	-19.155419, 13.923416
K1612	-19.141465, 13.929707	-19.142084, 13.927646
P1623	-19.144190. 13.917727	-19.146010, 13.906987
P1624	-19.139041, 13.923587	-19.137239, 13.921058
K1613	-19.136965, 13.928320	-19.136474, 13.925256
P1626	-19.127551, 13.932627	-19.122529, 13.929972
P1505	-19.128618, 13.940824	-19.124026, 13.934498
P1010	-19.122613, 13.935774	-19.120036, 13.932394
S1607	-19.121332, 13.939841	-19.116725, 13.936214
S1606	-19.117758, 13.942891	-19.114927, 13.937278
P1506	-19.108349, 13.947495,	-19.107967, 13.945064
S1605	-19.106653, 13.949596	-19.106884, 13.942732
P1001	-19.104872, 13.948053	-19.103075, 13.944063
P5	-19.089825, 13.953494	-19.074704, 13.949958

[1]Supplemental Table S1. Coordinates of measured columnar sections. Please visit http://doi.org/10.1130/GES01457.S1 or the full-text article on www.gsapubs.org to view Supplemental Table S1.

Table S2. Carbonate lithofacies

Lithofacies	Descriptions	Depositional environments
Microbialaminite	Undulose crinkly lamination with micro-unconformities, grainstone lenses, edge-wise intraclastic conglomerate, channels, tepee structure and tepee breccia, paleo-calcrete, silcrete or ferricrete	Littoral and supralittoral zones
Grainstone	Well-sorted arenite, generally oolitic or intraclastic, beds >0.2 m thick, commonly crossbedded, intraclast breccia, authigenic chert nodules	Shallow sublittoral and lower littoral zones, wave-dominated shoreface, off-shore sand bars
Stromatolite	Discrete columnar or domal, internally-laminated microbialite, with or without branching, generally associated with grainstone	Euphotic zone of sublittoral shelf and lower littoral zone
Ribbonite	Wavy-laminated lutite, beds <0.2 m thick, low-angle cross-stratification, wave or current ripples may be present	Open shelf and upper slope, above fairweather wave-base
Marly ribbonite	Argillaceous lutite, beds <0.2 m thick, low-angle cross-stratification, wave or current ripples, lenticular stratification	Deep shelf and upper to middle slope, above storm wave-base
Rhythmite	Flat parallel-laminated lutite or marl, with or without turbidites or debrites	Restricted deep shelf, lower slope and basin floor

[2]Supplemental Table S2. Carbonate lithofacies. Please visit http://doi.org/10.1130/GES01457.S2 or the full-text article on www.gsapubs.org to view Supplemental Table S2.

Lechte and Wallace, 2016) relative to other formations of the Otavi Group, but post-depositional Fe mobilization—Liesegang banding and fracture- or cleavage-controlled Fe mineralization are ubiquitous—frustrates attempts to discern the original distribution of Fe within the Chuos Formation.

The Chuos Formation is conformably but sharply overlain by the Rasthof (a.k.a. Berg Aukas) Formation, a distinctive Sturtian "cap carbonate" sequence composed of dark-gray turbiditic limestone, sublittoral microbialitic dolomite, and pale-gray shoreface dolarenite, the latter mapped separately as the Gauss Formation in the eastern Otavi belt (Hoffmann and Prave, 1996; Hoffman et al., 1998b; Yoshioka et al., 2003; Miller, 2008; Pruss et al., 2010; Dalton et al., 2013; Le Ber et al., 2013, 2015; Wallace et al., 2014). The sharp but conformable basal contact between disjunct facies—glacigenic and neritic nondetrital carbonate—is not an aberration. It is observed globally at the Sturtian glacial termination (Kaufman et al., 1997; Kennedy et al., 1998; Bold et al., 2016) and can be accounted for in the context of the Snowball Earth hypothesis (Hoffman and Schrag, 2002; Higgins and Schrag, 2003; Ridgwell et al., 2003; Fabre et al., 2013; Rooney et al., 2014). Where the Chuos Formation is absent, the base of the Rasthof Formation is a disconformity or unconformity on preglacial rocks. The Chuos-Rasthof couplet forms the base of the Abenab Subgroup, the middle division of the Otavi Group carbonate succession (Fig. 2).

On the Otavi platform (Fig. 2), the Chuos-Rasthof couplet is overlain by up to 500 m of peritidal carbonate-dominated cycles of the Gruis and Ombaatjie Formations. North-south crustal stretching, manifested by northward shedding of debris aprons eroded from the dip slopes of rift shoulders, occurred intermittently until the depositional onset of the Ombaatjie Formation (R-S surface in Fig. 2), after which passive-margin subsidence ensued. In the south, the Abenab Subgroup is thinner and more basinal in character, presumably reflecting a greater degree of crustal stretching south of the platform. A thin Rasthof Formation in the south is overlain by up to 350 m of parallel-laminated argillite and siltstone of the Narachaams Formation, which includes bundles of carbonate turbidites. The overlying Frannis-Aus Formation is a coarsening-upward stack of carbonate turbidites and debrites, culminating in coarse-grained oolite-clast debrite. It represents a falling-stand wedge leading into the Marinoan Glaciation (Hoffman, 2011). The Abenab Subgroup is overlain disconformably by the Tsumeb Subgroup, which has at its base the Marinoan glacial diamictite–cap carbonate couplet, the Ghaub and Maieberg Formations, respectively (Fig. 2).

The sub-Chuos successions are also different in the north and south, and between them is a paleo-high where the Chuos or Rasthof Formation lies directly upon the crystalline basement unconformably (Fig. 2). The sub-Chuos succession in the north is the Ombombo Subgroup, in which up to 650 m of cyclic peritidal dolomite (Devede Formation) is intercalated with and overlain by up to 400 m of cannibalized dolomite-chert conglomerate, sandstone, and fine-grained syn-rift clastics (Okakuyu Formation). A tuff near the top of the Devede Formation contains igneous zircons dated at 759 ± 1 Ma by U-Pb isotope-dilution thermal-ionization mass spectrometry (ID-TIMS) (Halverson et al., 2005).

In the south, syn-rift clastics are associated with bimodal volcanics of the Naauwpoort Formation, which contain igneous zircons dated in different areas by U-Pb sensitive high-resolution ion microprobe at 757 ± 5 Ma (Nascimento et al., 2016), and by U-Pb ID-TIMS at 747 ± 2 Ma and 746 ± 2 Ma (Hoffman et al., 1996). In the Summas Mountains, the younger volcanic area, the Naauwpoort Formation is overlain by up to 750 m of mixed peritidal dolomite and syn-rift clastics of the Ugab Subgroup (Guj, 1974; Miller, 1980, 2008).

The map distribution of the Otavi Group in our study area is largely controlled by the triangular Kamanjab inlier (Fig. 3), a foreland basement antiform situated at the confluence of two late Ediacaran orogenic belts, the SSE-striking Kaoko belt and WSW-striking Damara belt (Miller, 2008). The first of our case studies is situated on the western flank of the inlier near its northern apex (Fig. 3), corresponding to the northern or inner part of the Otavi Group carbonate platform (Fig. 2). The second case study involves a pair of structural domes, interpreted as interference folds (Maloof, 2000), at the junction of the two belts (Fig. 3). The Naauwpoort volcanics are not exposed in the domes, but up to 650 m of mixed syn-rift clastics and peritidal carbonate predating the Chuos Formation are inferred, on the basis of carbon isotopes, to be partly coeval with and partly younger than the Ugab Subgroup of the Summas Mountains. Despite strong lithological resemblance, the sub-Chuos in the domes is not an isotopic match for the Devede Formation in the case 1 area (Hoffman and Halverson, 2008; K.G. Lamothe, unpub. data). The third case study is situated on the southern flank of the Kamanjab inlier (Fig. 3), on the paleo-high (Huab ridge) where pre-Chuos cover strata are mostly absent (Fig. 2). Case 3 is structurally autochthonous with respect to Kamanjab basement, whereas case 1 is parautochthonous and case 2 is allochthonous.

There is no direct paleomagnetic constraint on Sturtian paleogeography from the Congo craton. In time-dependent global paleogeographic models, the Otavi platform is in the southern subtropics during Sturtian time (Trindade and Macouin, 2007; Li et al., 2013), consistent with carbonate-dominated pre- and post-Sturtian sedimentary facies (Fig. 2), which indicate relatively warm surface waters where carbonate oversaturation is highest. A Southern Hemisphere paleo-location is consistent with left-turning of upwelling bottom waters, inferred from consistently westward-directed (present coordinates) contourites in the Rasthof Formation and other formations of the foreslope zone (Fig. 2) (Hoffman and Halverson, 2008). A subtropical paleolatitude would have placed the Otavi platform in the zone of maximum net accumulation of ice in a Snowball Earth climate (Pierrehumbert et al., 2011; Abbot et al., 2013) but in the zone of maximum net ablation of ice in climates with open water at the equator (Abbot et al., 2011; Rose, 2015).

METHODOLOGY AND SEDIMENTARY LITHOFACIES

Selection of the study areas was based on previous reconnaissance stratigraphy (Hoffman and Halverson, 2008). Columnar sections were chosen from Google Earth satellite images and measured bed by bed to the nearest 0.1 m normal to bedding with a folding scale. Coordinates for the base and top of each section are given in Supplemental Table S1[1]. Carbonate rocks were classified according to the scheme outlined in Supplemental Table S2[2], and terrige-

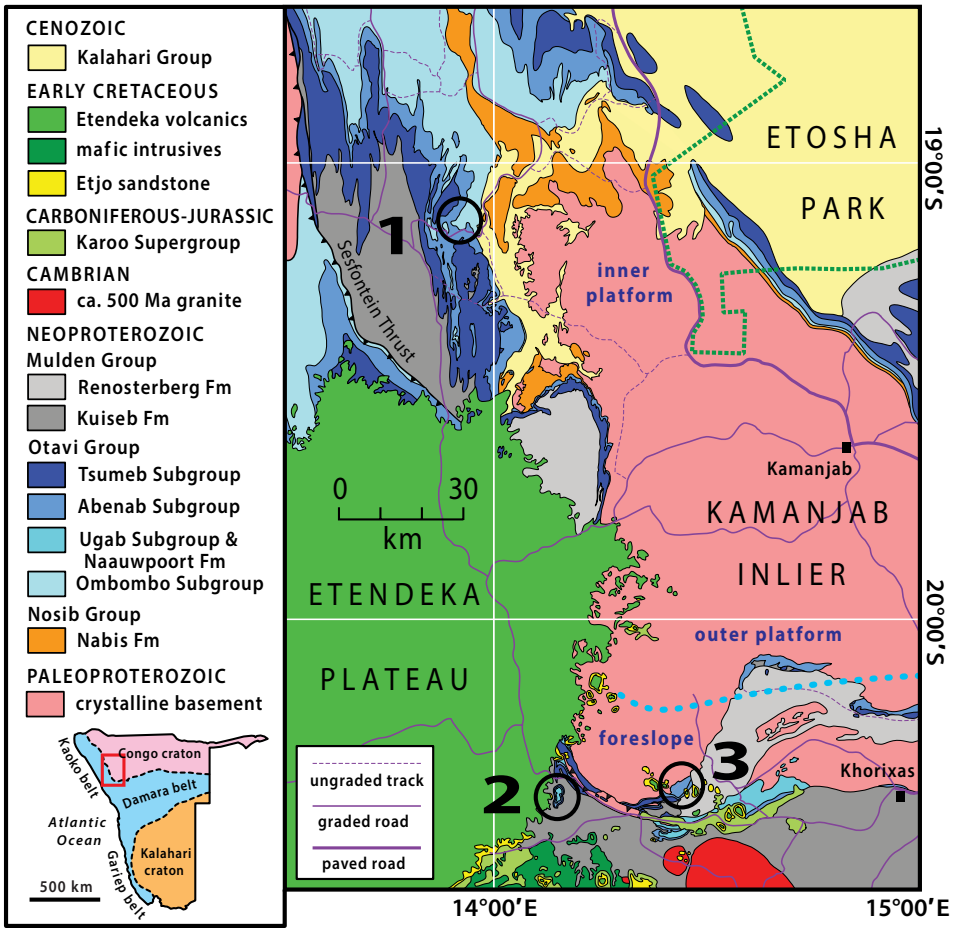

Figure 3. Geological map of deformed Neoproterozoic and flat-lying Phanerozoic cover units around the western part of the Kamanjab basement inlier (modified from Miller and Schalk, 1980). Red rectangle in the inset gives the map location on a tectonic map of Namibia. Paleogeographic zones of the Otavi Group (Fig. 2) carbonate platform are indicated in blue lettering. Dotted blue line is the platform-foreslope break. Case study areas are circled and numbered 1–3.

Table S3. Terrigenous lithofacies

Lithofacies	Descriptions	Depositional environments
Massive diamictite	Unstratified, sheared or unsheared, wackestone with matrix-supported heterolithic pebbles and boulders, generally subrounded, faceted and striated clasts	Subglacial and ice-proximal subaqueous settings, lodgement-, sublimation- and melt-out tills, in some cases redeposited downslope
Stratified diamictite	Laminated and bedded suspension fallout containing outsized dropstones with impact-related features (e.g., punctured layers, raised rims, overturned flaps), turbidites and debrites, slumps and cryokinetic structures	Subaqueous periglacial, ice grounding-zones particularly of ice streams, proximal ice-shelf rafting, far-travelled iceberg rafting, hypopycnal suspension plumes
Sorted diamictite	Well-sorted arenite or fine-grained rudite containing outsized dropstones, climbing ripples, crossbedding, commonly channelized within massived diamictite or as wedges within stratified diamictite	Sub- and intraglacial melt-water tunnels, grounding-line tunnel-mouth fans, sub-ice shelf tidal channels
Conglomerate	Clast-supported rudite, clasts subrounded to well-rounded, generally stratified with sand-rich lenses and zones, graded or reverse graded, paleo-calcrete	Alluvial fans and steep-gradient rivers, proglacial outwash (sandur)
Sandstone	Grain-supported arenite, generally well-bedded, commonly crossbedded, ripple marks, current lineation, pebble lags and lenses may be present	Aeolian, riverine, deltaic, and wave- or tide-dominated coastal systems, off-shore bars, slope channels and fans
Siltstone	Grain-supported siltstone, generally thin-bedded, may be interstratified with fine-grained sandstone and/or argillite, low-angle cross-stratification, wave or current ripples, turbidites, mudcracks if desiccated	Riverine levees and deltas, open and semi- restricted shelves, slope-channel levees and fans
Argillite	Terrigenous mudrock, massive to foliated, parallel-sided laminae, terrigenous or carbonate turbidites, authigenic sulfide and carbonate	Lakes, coastal lagoons, restricted shelves, basin floors

[3]Supplemental Table S3. Terrigenous lithofacies. Please visit http://doi.org/10.1130/GES01457.S3 or the full-text article on www.gsapubs.org to view Supplemental Table S3.

nous, including glacigenic, rocks, as in Supplemental Table S3[3]. The nature of the basal contact of each bed or measured unit was noted. Care was taken when measuring in drainages, which are commonly situated on faults. Remeasured sections indicate better than 95% reproducibility in thickness, but a degree of inter-operator error in rock classification is inevitable, given differences in prior experience.

CASE 1. BEDROCK TROUGH AT OMUTIRAPO SPRINGS

Freshwater springs and associated travertine deposits are localized by steeply dipping growth faults in the lower Otavi Group. Near the currently unoccupied village of Omutirapo (19°07.184′S, 13°56.808′E), an east-striking, south-side-down growth fault cuts the Ombombo Subgroup, which is tilted westward between 25° and 50° (Figs. 4, 5). The growth fault has a stratigraphic offset of ~160 m, but the sub-Chuos erosion surface shows no displacement across the fault trace (Fig. 5), suggesting that fault slip had ceased before the erosion surface formed. Although the bedrock trough removed the critical contacts, the growth fault appears to have been most active after the Devede and before the Okakuyu Formations were laid down (Fig. 6).

Directly north of the growth fault, the subglacial erosion surface at the base of the Chuos Formation cuts stratigraphically downward from north to south at the expense of the Okakuyu and Devede Formations (Figs. 5–7). The depth of erosional downcutting is nearly 400 m over a horizontal north-south distance of 1.2 km, with over one-half of the drop occurring in just 150 m (Fig. 7). Inci-

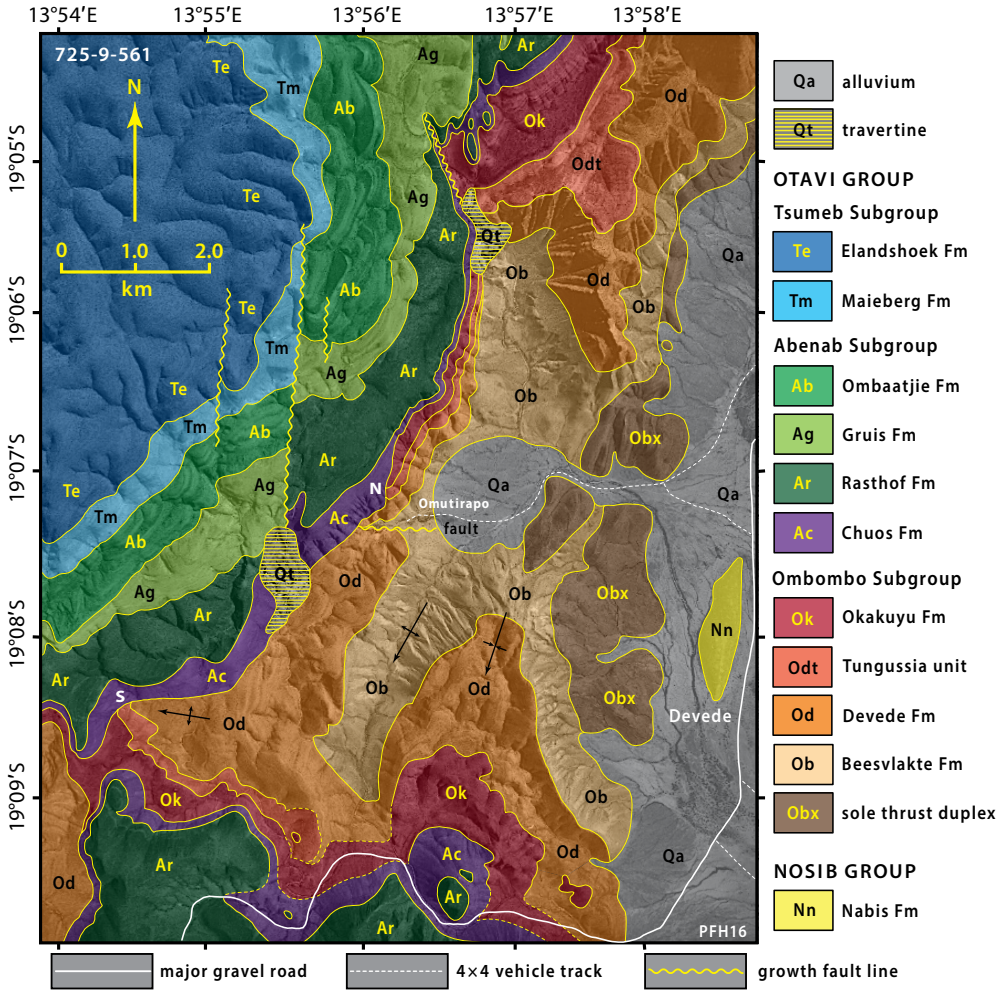

Figure 4. Geology on the western flank of Kamanjab inlier around Omutirapo springs (for location see Fig. 3, case study area 1), superimposed on aerial photograph 725-9-561 (Namibian Ministry of Lands and Resettlement, Windhoek). The north and south walls of the U-shaped glacial paleovalley filled by Chuos Formation (unit Ac) are labeled "N" and "S" respectively, and the south-side-down growth fault stratigraphically beneath the paleovalley near Omutirapo is labeled "fault". Although gently dipping, the entire Otavi Group carbonate succession is allochthonous relative to the underlying Nosib Group subarkose, separated by an imbricate thrust duplex (unit Obx) within the lower and middle Beesvlakte Formation. By coincidence, Omutirapo topographically occupies a Carboniferous glacial cirque, which emptied eastward into a south-flowing tributary to a westward-flowing ice stream within the Gondwanan ice dome centered on southern Africa (Martin, 1961, 1968). The whaleback outcrop of Nosib Group subarkose directly north of Devede is an apparent Carboniferous glacial landform. The travertine parapet at the north end of the cirque is localized on an east-side-down growth fault of late Ombombo Subgroup age, which was inverted as a west-side-down growth fault in late Rasthof Formation time (Hoffman and Halverson, 2008).

sion of the Ombombo Subgroup is quantitatively reciprocated by thickening of the glacigenic Chuos Formation (Fig. 7).

The Chuos Formation consists of interlayered massive, sheared and stratified diamictites (Figs. 8A, 8B, 8E), with discontinuous bodies of conglomerate, pebbly sandstone, and siltstone (Fig. 8C), with or without ice-rafted debris (Fig. 6). We concur with the interpretation of Le Heron et al. (2013a) that the diamictites are subglacial ice-contact deposits, but the discontinuous nature of the associated facies is consistent with transient meltwater cavities beneath the ice sheet (e.g., Buechi et al., 2017) as opposed to a global interglacial stage (Le Heron et al., 2013a). Conglomerate and pebbly sandstone represent connected cavities with flowing meltwater, while laminated siltstone (Fig. 8C) indicates cavities with ponded meltwater. Meltwater ponding may occur where a reverse bed slope exists downstream (Buechi et al., 2017).

The sub-Chuos incision and onlap relationships (Fig. 7) north of the growth fault were known previously (Hoffman and Halverson, 2008; Le Heron et al., 2013a), but the width of the incision was unknown. We have now mapped the opposite (northward-facing) side of the incisement (Figs. 4, 5, 9) and constrained its shape with columnar sections (Fig. 6A). It has steep sides and a broad floor, with an axial depth of ~450 m and a brim width of 4.3 km in the line of exposure, or 3.0 km projected onto a plane oriented north-south (003°

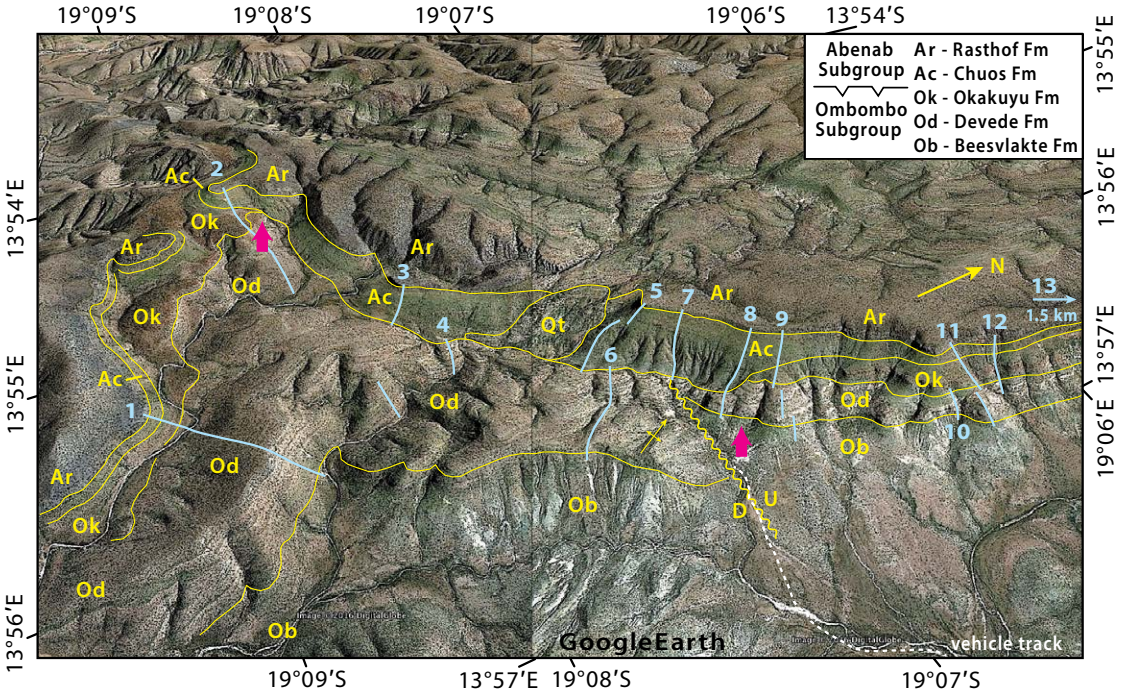

Figure 5. Inclined satellite view of the incised Sturtian paleovalley at Omutirapo springs, looking toward the WNW. Magenta arrows indicate the paleovalley walls, 4.3 km apart, defined by the erosive base of the glacigenic Chuos Formation (unit Ac). Wavy line is an intra–Ombombo Subgroup (Tonian) growth fault, which may have localized Sturtian incision. Chuos Formation is 500 m thick in the paleovalley axis (Fig. 7), 10× thicker than outside the paleovalley. Units above the Rasthof Formation (Fig. 4) are not shown for simplicity. Numbered light-blue lines are the measured sections of Figure 6. Unit Qt—Quaternary travertine as in Figure 4.

azimuth) normal to the trace of the growth fault (Fig. 5). Its transverse dimensions lie within the normal range for subglacial bedrock troughs in Antarctica, Greenland, and areas bordering the European Alps (Cook and Swift, 2012; Patton et al., 2016). Was the incisement cut by glacial ice or running water?

In 1904, the leading German geomorphologist and Quaternary geologist Albrecht Penck was invited by his American counterpart T.C. Chamberlin to summarize his reasons for interpreting many surface features in and around the Alps as being of glacial origin. He began his paper (Penck, 1905) by observing that the shapes of Alpine valleys are not like those eroded by rivers. He wrote that in transverse profile:

> The cross-sections of our Alpine valleys are also other than what one might expect [for river-cut valleys]. The master-valleys have in general an extended flat bottom, at the sides of which rise steep walls. At a certain height, steep slopes below change into more gentle ones above. Well-marked ledges separate the two slopes, and form distinct shoulders on both sides of the valley—a condition not usually found elsewhere.

This is an accurate description of our true-scale profile of the Chuos paleovalley at Omutirapo springs (Fig. 6A). The Alpine comparison is not inappropriate as the area was tectonically active during the Sturtian glaciation (Hoffman and Halverson, 2008).

Many more columnar sections are needed to fully characterize the synglacial deposits (Fig. 6B). Although massive and sheared diamictites are the predominant lithologies (Figs. 8A, 8B), the direction of ice flow remains unknown. Clast fabric analysis has not been undertaken, and a small number of paleocurrent measurements from rare cross-bedding and current ripples in sandstone give ambiguous results (Fig. 6B). Units of sorted sediment—conglomerate, sandstone, and siltstone (Fig. 6B)—are common within the trough (columnar sections 3–11, Fig. 6B) but rare outside of it (sections 1–2 and 12–13). Subsurface investigation of bedrock troughs related to Pleistocene glaciation of the Alps indicates that sorted deposits are most abundant in overdeepenings, subglacial troughs that shallow axially in the downstream as well as upstream directions (Buechi et al., 2017; Patton et al., 2016). This observation led to the hypothesis that ice-bed separation, creating meltwater cavities in which subglacial sorted deposits accumulate, is favored by hydraulic overpressuring associated with overdeepenings eroded into bedrock aquitards (Buechi et al., 2017). In the case of Omutirapo trough, it may not be correct to assume that the bedrock was an aquitard if the location and trend of the trough was controlled by fault damage associated with the pre-Chuos growth fault (Fig. 6B). At this point, however, a causal fault-trough relationship at Omutirapo springs is conjectural.

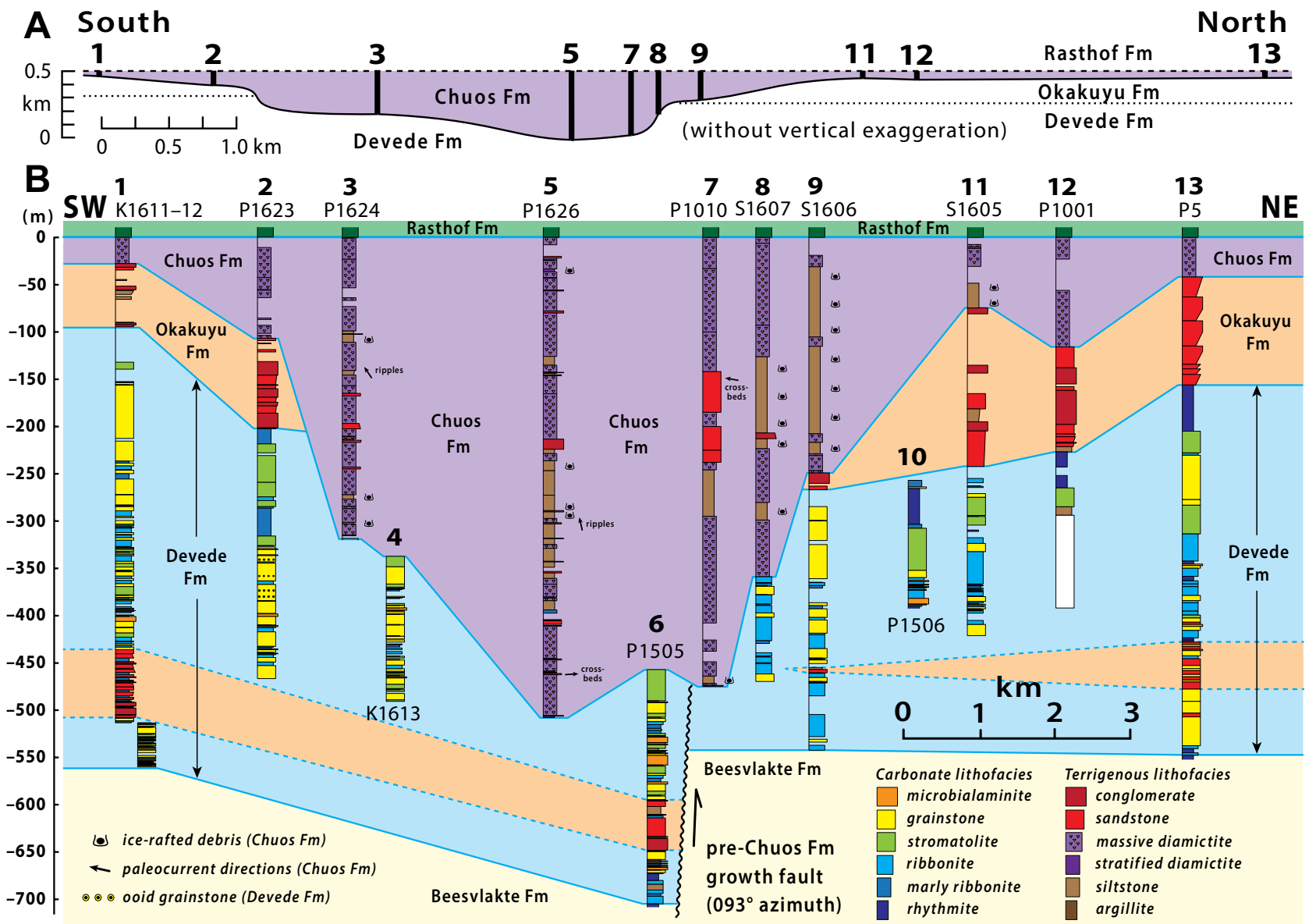

Figure 6. Columnar sections of the Ombombo Subgroup (Beesvlakte, Devede, and Okakuyu Formations) and Chuos Formation in the Omutirapo springs area, documenting incision of the Sturtian paleovalley. Vertical datum (0 m) is the base of the Rasthof Formation cap carbonate. (A) Chuos Formation sections (see Fig. 5 for locations) projected without vertical exaggeration onto a 003° azimuth, or normal to the pre-Chuos growth fault between sections 6 and 7 shown in B. (B) Sections positioned schematically along the SSW–NNE outcrop belt (Fig. 4) with 12.3× vertical exaggeration to show lithologic units (described in Supplemental Tables S2 [footnote 2] and S3 [footnote 3]). Field number for each section is shown beneath the column number. The white box in column 12 is undifferentiated dolostone. The orange band within the Devede Formation is a sandstone-conglomerate lithosome.

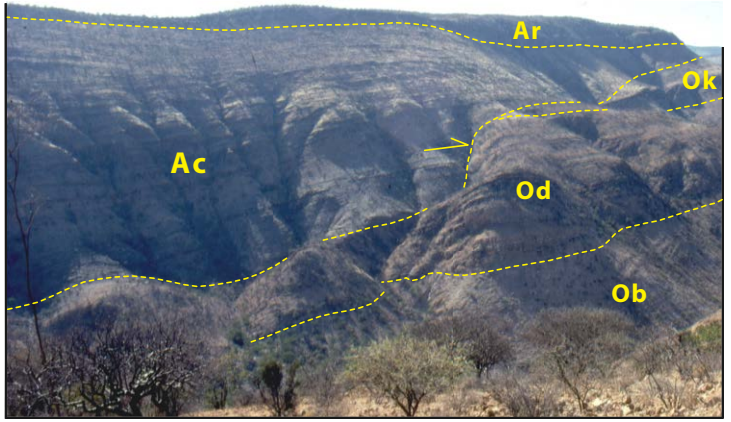

Figure 7. North wall of the Omutirapo paleovalley, viewed from the south. Chuos Formation (unit Ac) thickens southward from 65 to 450 m in the field of view, incised into the Okakuyu (unit Ok) and Devede (unit Od) Formations. Beesvlakte Formation is unit Ob; Rasthof Formation is unit Ar. Note the onlap of Chuos glacial and associated strata against the steep valley wall (half arrow).

CASE 2. COMPOSITE MORAINE IN THE VREDE DOMES

A pair of allochthonous structural domes (Fig. 10) on the west bank of the Huab River on Vrede farm provide excellent three-dimensional exposure of the Otavi Group in the basin zone (Fig. 2) over an area of ~15 km^2. The domes are part of a larger area systematically mapped by Frets (1969) and were specifically investigated by Maloof (2000), who interpreted the domes as interference folds, related to east-west and subsequent north-south shortening during formation of the Kaoko and Damara belts, respectively (Coward, 1981; Passchier et al., 2016). Intersecting cleavages (Fig. 11A) are among the evidence supporting this interpretation (Maloof, 2000). Neither the Naauwpoort volcanics nor crystalline basement is exposed in the domes: the structurally deepest unit in the south dome is a limestone marble tectonite (Fig. 10).

Ugab Subgroup in the Vrede Domes

The cores of both domes are composed of coarse-grained syn-rift clastics and peritidal carbonates of the Ugab Subgroup (Fig. 12). In a remarkable facies change, cobble and boulder conglomerate of alluvial origin in the north pass laterally into oolitic, stromatolitic, and wave-rippled micritic dolostone of coastal marine origin in the south. The facies change takes place over a horizontal distance (not corrected for folding) of 5 km. Southward-tapering clastic tongues backstep northward over time (Fig. 12), reflecting progressive marine invasion attributable to crustal stretching and subsidence.

A mappable flooding surface, where decameters of ribbony dolomicrite sharply overlie oolitic grainstone and/or columnar stromatolite (tungussiform) type of Hofmann [1969], characterized by strongly divergent branching), provides a reference horizon and datum near the top of the Ugab Subgroup (Fig. 12). The glacial erosion surface at the base of the Chuos Formation (Fig. 11A) lies between 10.1 m (column 12, Fig. 12) and 76.5 m (column 1) above this flooding surface.

Abenab Subgroup in the Vrede Domes

The Ugab Subgroup in both domes is mantled by the Abenab Subgroup (Fig. 13), which comprises the syn-glacial Chuos Formation, a thin Rasthof Formation cap dolomite, and the argillaceous Narachaams Formation.

The Chuos Formation is highly variable in thickness (Fig. 13). In the southwestern half of the south dome (columns B–K, Fig. 10), it swells to a maximum thickness of 223 m, compared with a median and average thickness of only 6 m elsewhere in the domes (Fig. 13). Thickening of the Chuos Formation appears to be bilateral in the diagram, but this is an artifact of curvature in the line of columnar sections (Figs. 10, 12–16). The simplest interpolation is that of a southwestward-thickening wedge. The thickened sections are complex in detail (Figs. 13, 16), made up, in decreasing order of abundance, of massive silicate-clast diamictite, massive carbonate-clast diamictite, stratified silicate-clast diamictite, clast-free argillite, and clast-supported conglomerate. In the north dome, massive carbonate-clast diamictite is relatively more abundant. The Chuos Formation everywhere overlies a disconformity. The directly underlying dolomite is fractured and locally brecciated, while pockets of locally derived debris underlie the basal polymictic diamictite (Fig. 11B).

The Rasthof Formation conformably overlies the Chuos Formation everywhere except in columns E–G, where it is truncated by the Marinoan glacial surface (Figs. 13, 14). The base and top of the Rasthof Formation are sharp and its thickness is rather uniform, averaging 2.4 m with extremes of 0.6 and 4.3 m. A discontinuous basal interval (0.2–0.3 m thick) of ribbony dolomite, olive-tan in color, grades into a characteristic charcoal-black, finely laminated dolomite, easily recognizable in float. Evidence of subaerial exposure is lacking, but small-scale irregularities and crinkling suggest a subaqueous microbial origin for the lamination. This is supported by excellent examples of rollup structures (Pruss et al., 2010) in column S (also present in column K), implying that the laminae were pliable but cohesive at the sediment-water interface. This would only have been possible if the carbonate grains were interwoven with microbial filaments and extracellular polymeric substances. The Rasthof Formation is everywhere overlain sharply but conformably by argillite of the basal Narachaams Formation (Fig. 13). No unit lithologically resembling the Rasthof Formation occurs within either the Chuos or the Narachaams Formations. Maloof (2000) highlighted the Rasthof Formation in the Vrede domes as a key stratigraphic marker for distinguishing the two Cryogenian glacial formations (Figs. 13, 14).

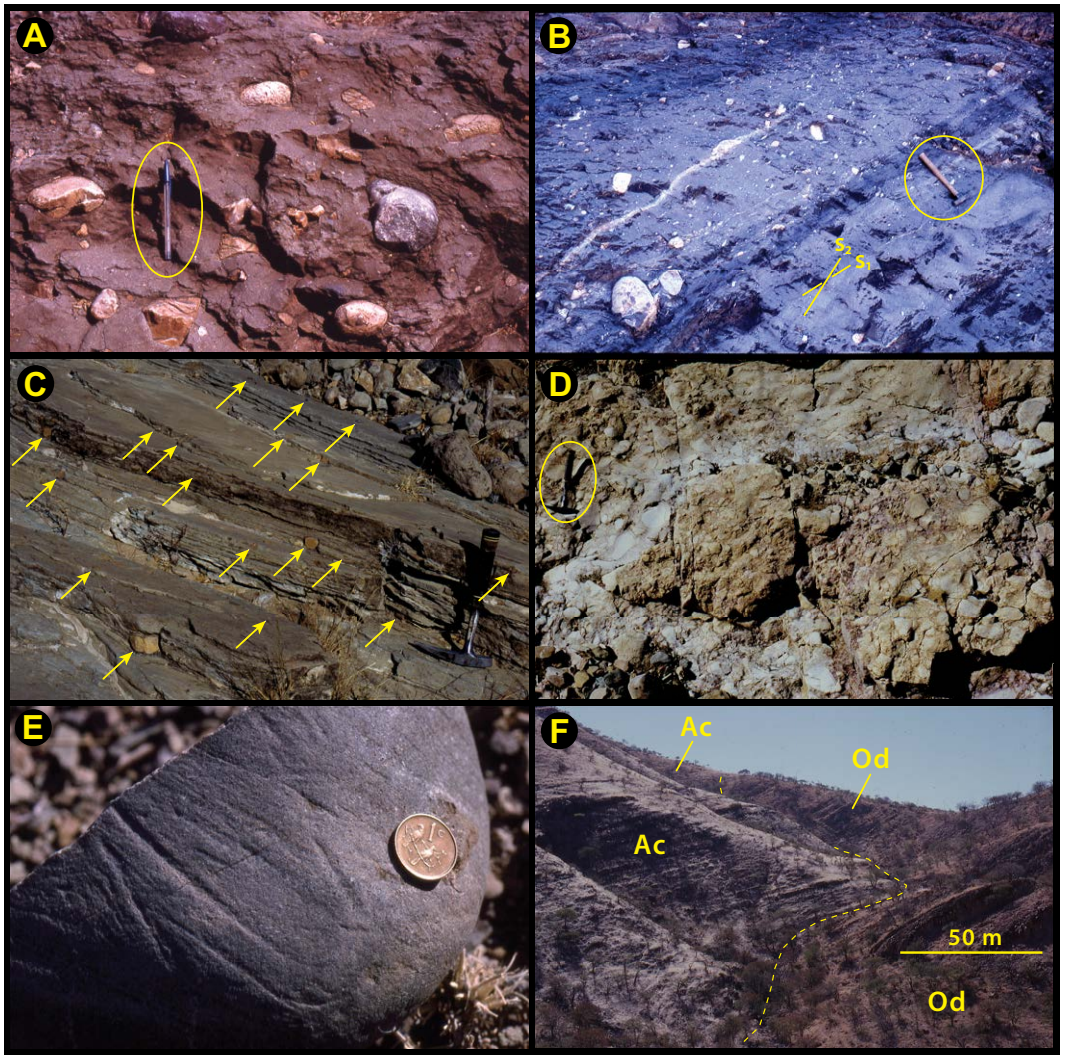

Figure 8. Field images from the Omutirapo springs area. See Figures 5 and 6 for column locations. (A) Massive diamictite with clasts of dolomite, quartz arenite, and basement grantitoid; Chuos Formation, column 7. Pen (circled) is 15 cm long. Note the subrounded clasts, consistent with subglacial (not supraglacial) transport. (B) Sheared diamictite in which soft-sediment shear banding (S_1) is transected by tectonic cleavage (S_2); Chuos Formation, column 7. Hammer handle is 33 cm long. (C) Laminated siltstone with ice-rafted dropstones (arrows) of dolomite and quartz arenite; Chuos Formation, column 7. (D) Monomict breccia and conglomerate of stromatolitic dolomite from the directly underlying Devede Formation forms the basal meter of the Chuos Formation in the paleovalley; column 7. (E) Quartz-arenite cobble with multiple directions of glacial striae from a massive diamictite high in section; column 5. Coin is 2 cm in diameter. (F) Looking north toward the north wall of the paleovalley between columns 7 and 9. Dashed line is the incisement surface. Chuos Formation (unit Ac) in foreground is directly on strike with Devede Formation (unit Od) dolomite in background.

The Narachaams Formation consists of argillite, argillite with graded siltstone laminae (Fig. 11C), and argillite with spaced, 1–10-cm-scale dolomite or limestone turbidites (Fig. 11D). Authigenic carbonate occurs as ankeritic(?) concretions up to 1.0 m in diameter. Certain argillite units are rich in finely disseminated authigenic pyrite. The Narachaams Formation conformably overlies the Rasthof Formation and disconformably underlies the Tsumeb Subgroup. Its thickness ranges from 0 to 237 m within the domes (Fig. 13). Three factors potentially account for the large variability: depositional onlap against the Chuos diamictite, variable truncation beneath the sub-Tsumeb glacial disconformity, and tectonic strain of the rheologically weak argillite during formation of the structural domes. Tectonic thickening of the Narachaams Formation in section M could be accommodated by tectonic thinning in sections N and O (Fig. 13). More detailed mapping (e.g., between columns M and N) is needed to evaluate these factors.

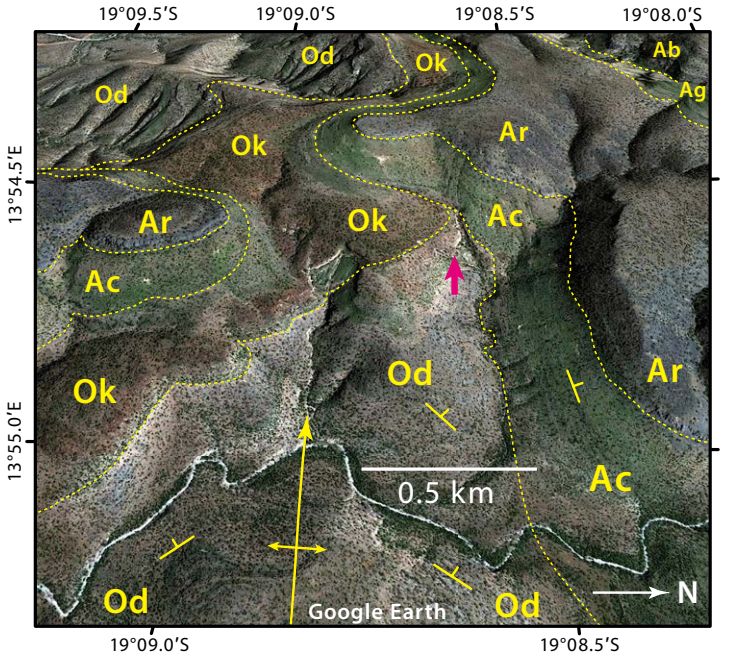

Figure 9. Inclined satellite view looking westward at the north-facing south wall of the Omutirapo paleovalley (see Figs. 4 and 5 for location). Magenta arrow indicates where the Chuos Formation (unit Ac) cuts down steeply across the Okakuyu (unit Ok) and upper Devede (Od) Formations (between columns 2 and 4, Figs. 5, 9). Other units: Ar—Rasthof Formation; Ag—Gruis Formation; Ab—Ombaatjie Formation.

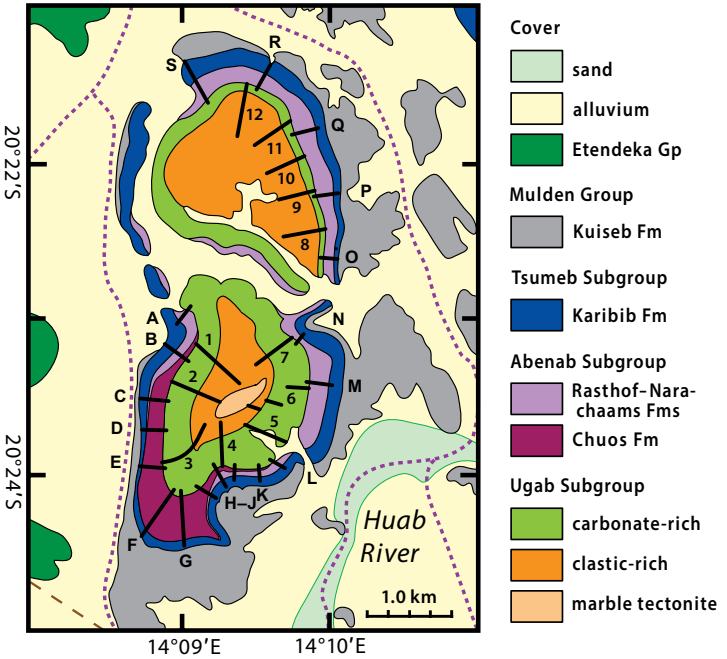

Figure 10. Stratigraphic geology of the Vrede domes, showing locations of columnar sections in Figures 12–13, 15–16. Vehicle tracks are indicated by purple dashed lines. Ugab Subgroup columns are numbered 1–12; Abenab Subgroup columns are lettered A–S. Mapping from Maloof (2000) and the senior author.

Tsumeb Subgroup in the Vrede Domes

The Marinoan glacigenic Ghaub Formation is poorly represented in the Vrede domes, reaching only 5.5 m in maximum thickness and missing altogether in columnar sections G, N, and O (Fig. 13). Where present, it has a sharp erosive contact with the underlying Abenab Subgroup and an abrupt conformable contact with the overlying Keilberg Member of the Maieberg Formation, the Marinoan "cap dolomite" sensu stricto. By convention, the base of the Keilberg Member corresponds to the base of the Ediacaran Period globally (Knoll et al., 2006).

In columnar section P (Fig. 13), 0.5 m of massive diamictite, in which subrounded clasts of dolomite and quartzite "float" in a dolomite wackestone matrix, is overlain by 2.6 m of parallel-laminated quartz siltstone with ice-rafted dropstones of quartzite and dolomite, the latter up to 24 cm in diameter. Thinner intervals of diamictite and/or siltstone with dropstones occur in columnar sections C, H, L, M, and Q–S. In section F, 2.0 m of stratified carbonate-clast diamictite with possible Rasthof-derived clasts lies sharply on polymictic diamictite of the Chuos Formation, derived from the Ugab Subgroup and the crystalline basement.

The 6–20-m-thick Keilberg Member (Fig. 13) is the basal transgressive unit of the Ediacaran Karibid Formation (Fig. 2). Its base is sharply conformable with the Ghaub Formation, or disconformable where the Ghaub is absent. It consists of pale-gray to pale pinkish-gray, tan-weathering, micropeloidal dolomite. The top of the Keilberg Member is gradational with deeper-water, marly limestone and/or dolomite rhythmite representing maximum postglacial flooding. In facies, the Keilberg Member in the Vrede domes is similar to the "distal foreslope" on Fransfontein Ridge, 75 km to the ENE (Hoffman et al., 2007)—tubestone stromatolite is absent and a zone of rumpled sheet cracks filled by fibrous, isopachous dolomite cement occurs close to (but not at) the base.

The Karibid Formation (Fig. 2) is the chemostratigraphic equivalent in the basin and foreslope of the 1.4-km-thick post-glacial Tsumeb Subgroup on the Otavi platform (Hoffman, 2011). It is divided into three members: the basal transgressive Keilberg Member, a marly middle member marking the maximum postglacial flooding stage, and an upper highstand tract composed of dolomite rhythmite and rhythmite intraclast slump breccia, variably dedolomitized.

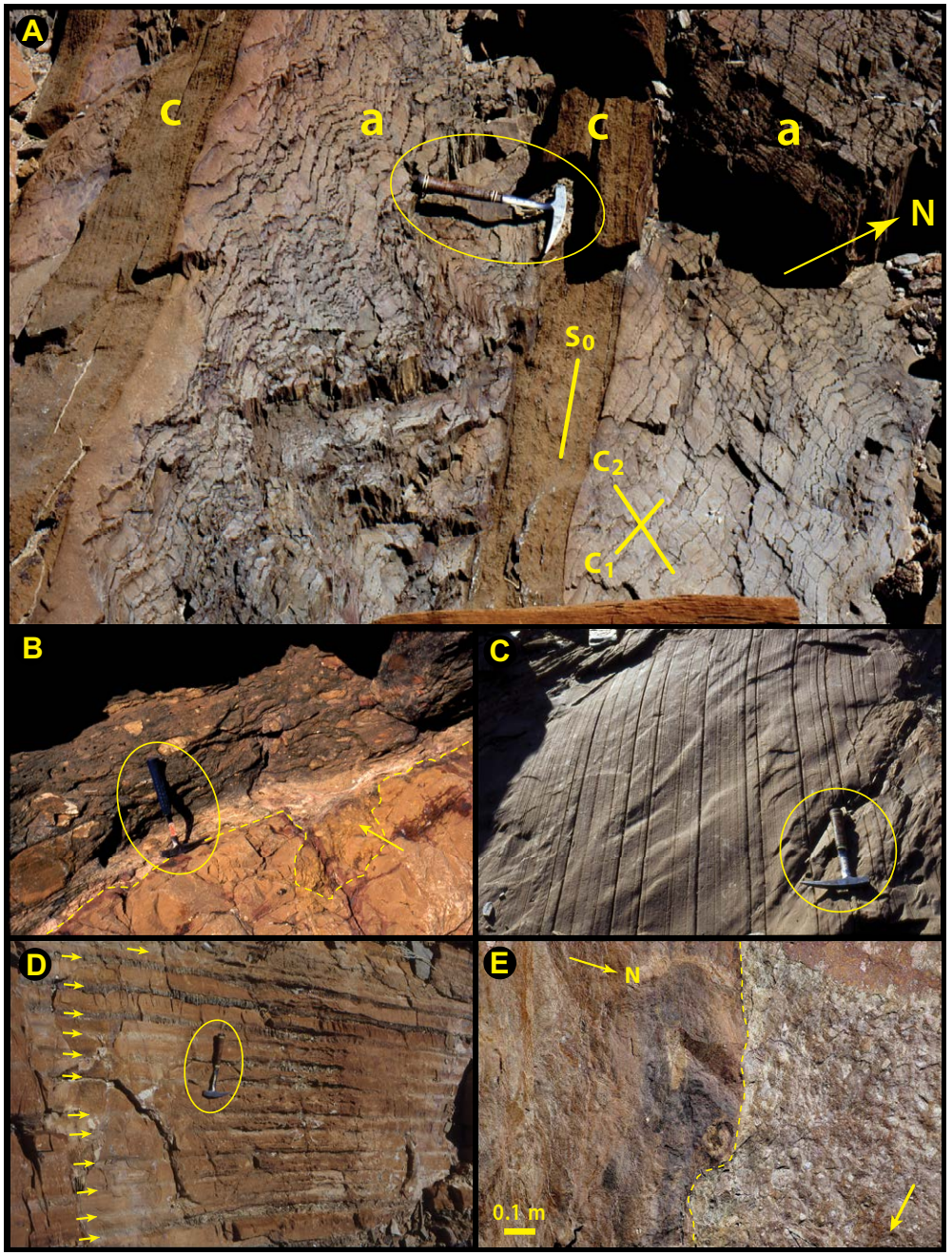

Figure 11. Field images from the Vrede domes and Toekoms half graben. (A) Intersecting cleavages in interbedded argillite (a) and carbonate (c) of the Narachaams Formation in the north dome (column R, Fig. 10) on Vrede farm. The older (C_1) and younger (C_2) cleavages are related to flattening in the Kaoko and Damara belts, respectively (Fig. 3). S_0 is primary layering. (B) Glacial erosion surface (dashed) between Chuos Formation diamictite (upper left) and Ugab Subgroup dolomicrite in the south dome (column K). Arrow indicates pocket of locally sourced lodgment tillite beneath farther-traveled heterolithic diamictite. (C) Narachaams Formation argillite with centimeter-scale siltstone turbidites in the north dome (column Q). Stratigraphic younging is to the right. Basinal facies dominate the Cryogenian nonglacial interlude south of the Otavi platform (Fig. 2). (D) Narachaams Formation argillite with limestone turbidites (arrows) in column R. (E) Sharp contact (dashed) between footwall basement orthogneiss (left) and Chuos Formation diamictite (right) at Toekoms border fault ~1.2 km stratigraphically above the top of the hanging-wall basement (Fig. 19). The basement is ferruginized, but there is little overt evidence of shear at the contact, despite ~1.3 km of inferred growth strata overlying this horizon. Arrow (lower right) indicates the stratigraphic younging direction.

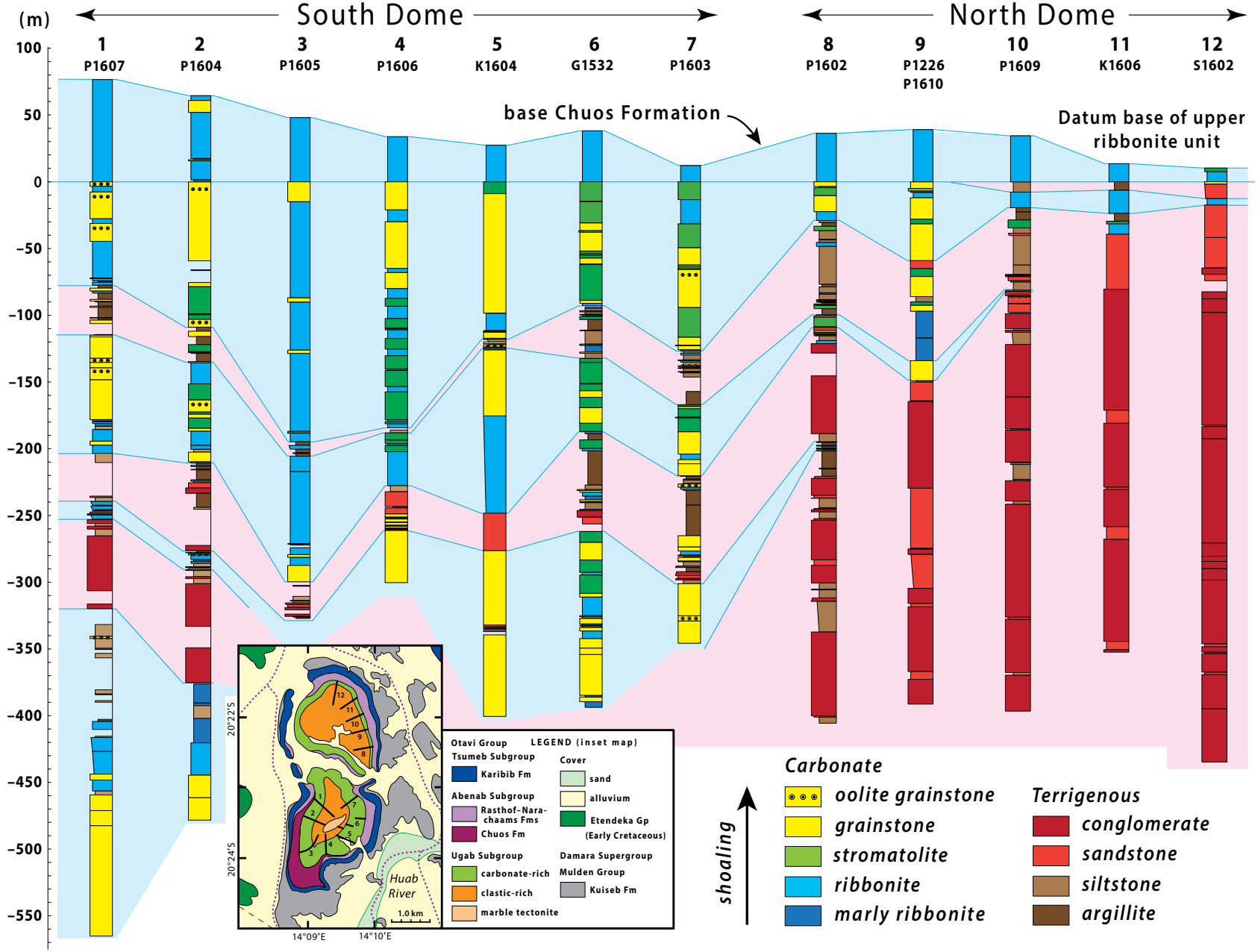

Figure 12. Columnar sections of the Ugab Subgroup in the Vrede domes. Sections 1–12 are ordered anticlockwise around the domes (see inset map and Fig. 10 for locations), minimizing the separation of adjacent sections. There is a major facies change from coarse-grained alluvial clastics in the north (column 12) to coastal marine carbonate in the south (columns 3–5), with northward backstepping of clastic tongues over time. Blue shade indicates predominant carbonate, pink shade predominant siliciclastic. Vertical datum (0 m) is a mappable flooding surface beneath the upper dolomite ribbonite unit and is used as a paleo-horizon (Figs. 15–16) for reconstructing the paleotopography of the sub-Chuos glacial erosion surface (Fig. 11B). Field number for each section is shown beneath the column number.

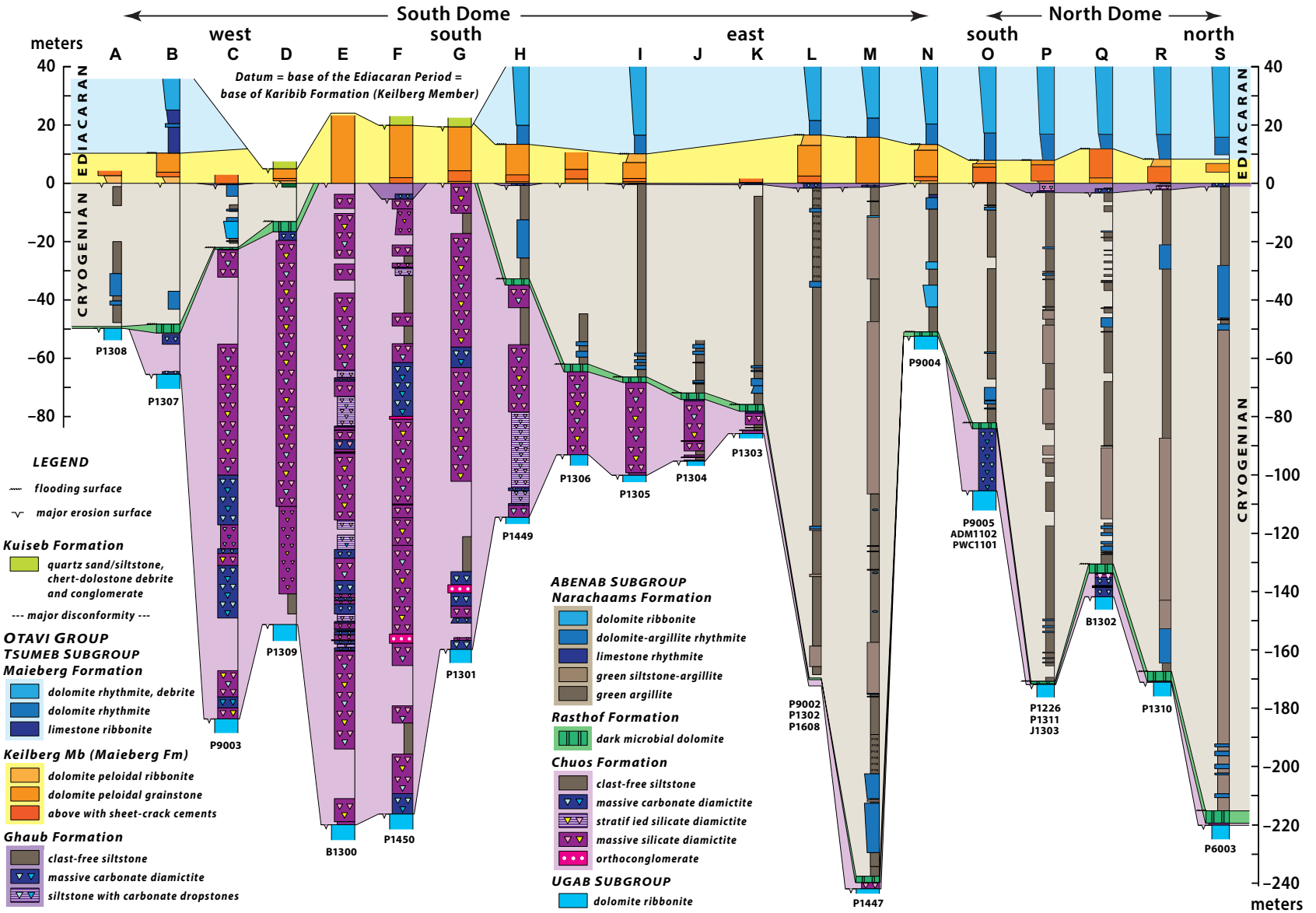

Figure 13. Columnar sections A–S of the Abenab and lower Tsumeb Subgroups in the Vrede domes. Columns are ordered anticlockwise around the domes (see Fig. 10 for locations). Vertical datum (0 m) is the base of the Keilberg Member (Karibib Formation), the Marinoan cap dolomite taken as the base of the Ediacaran Period (Knoll et al., 2006). The Chuos Formation thickening is a wedge, tapered to the northeast; the apparent lenticular shape is an artifact of the curved line of sections (Fig. 10). Note the thin Rasthof Formation cap limestone draping the diamictite wedge (Chuos Formation) in columns B–D and H–M. Note also the thin Ghaub Formation diamictite above a Marinoan glacial erosion surface that decapitated the Sturtian diamictite wedge in columns E–G. In column F, Marinoan and Sturtian diamictites are in contact; in column G, the Marinoan cap dolomite overlies the Sturtian diamictite. Unlike other units, the argillaceous Narachaams Formation has undergone significant compaction, which has not been decompacted in this figure. Field number for each section is shown beneath the column.

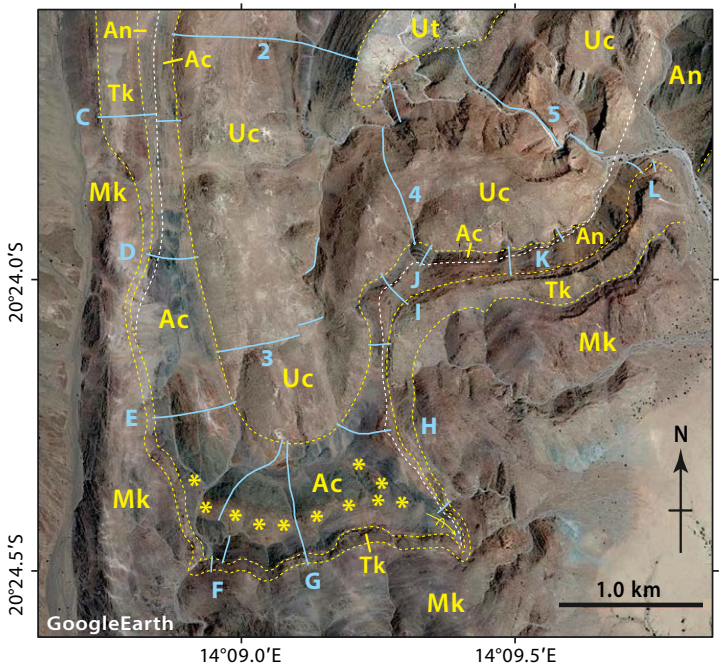

Figure 14. Vertical satellite view of the south end of the Vrede south dome, showing thickening of Sturtian diamictite in the Chuos Formation (unit Ac) and the locations of columnar sections 2–5 and C–L. White dashed line indicates the thin Rasthof Formation (cap limestone) draping the Chuos Formation, which is truncated by the Ediacaran Karibib Formation (unit Tk) in columns E–G. Other units: Ut—marble tectonite; Uc—carbonate-facies Ugab Subgroup; An—Narachaams Formation (Figs. 11C–11D); Mk—syn-orogenic Kuiseb Formation. As drawn, unit Tk includes up to 5.5 m of Marinoan diamictite (Ghaub Formation) as in column F (Fig. 13). The pale band indicated by asterisks in the upper Chuos Formation corresponds to carbonate diamictite in columns F and G (Fig. 16).

The Karibib Formation is heavily silicified beneath the disconformably overlying quartz arenite of the Kuiseb Formation. The Karibib Formation is significantly thinner in the Vrede domes, 5–127 m, compared with foreslope areas to the ENE (e.g., 327 m on Bethanis farm and 468 m at Fransfontein village). This is due partly to downslope condensation (columnar section S, Fig. 10) and partly to truncation beneath the sub–Kuiseb Formation disconformity. In sections D–G, this disconformity cuts all the way down to the Keilberg Member (Figs. 13, 16).

Kuiseb Formation (Mulden Group) in the Vrede Domes

Around the Vrede domes, the Kuiseb Formation (Fig. 10) consists of syn-orogenic feldspathic and non-feldspathic quartz-chert arenite, polymictic conglomerate, green argillite and siltstone, and argillite-hosted olistoliths and olistostromes of dolomite and chert, apparently derived from the Karibib Formation (Frets, 1969; Maloof, 2000; Schreiber, 2006). Recently, Nascimento et al. (2016) reinterpreted the Kuiseb Formation in the Vrede and adjacent areas as Cryogenian in age, equivalent to the Marinoan Ghaub Formation. This interpretation necessitates a thrust contact between the Karibib and Kuiseb Formations (Nascimento et al., 2016). It permits a glacial origin for the Ghaub Formation to be questioned (Nascimento et al., 2016), because the Kuiseb Formation olistostromes and olistoliths are not glacigenic. Here we follow earlier work (Frets, 1969; Guj, 1974; Miller and Schalk, 1980; Hoffmann, 1989; Stanistreet et al., 1991; Maloof, 2000; Miller, 2008) in interpreting the Karibib-Kuiseb contact as a regional-scale erosional disconformity, with no duplication of the stratigraphic sequence. In our view, the olistostromes and olistoliths of the Kuiseb Formation have no bearing on the origin of Cryogenian diamictite in the Chuos or Ghaub Formations.

Interpretation of the Chuos Formation in the Vrede Domes

The steep wedge of diamictite in the southwestern half of the south dome (Figs. 13, 14) does not coincide with any apparent incisement of the underlying Ugab Subgroup (Fig. 12). It should therefore represent a moraine-like body with positive synoptic relief (Figs. 15, 16). This is consistent with the increasing stratigraphic depth of Marinoan glacial erosion toward the apex of the buildup (Fig. 16), progressively truncating the Narachaams and Rasthof Formations. The post-Marinoan ca. 590 Ma erosion surface beneath the Kuiseb Formation also cuts stratigraphically deepest, down to the Keilberg Member, at the apex of the buildup (Figs. 13, 16).

In columnar sections E–G (Fig. 13), the Tsumeb Subgroup with its lithologically distinct Marinoan cap dolomite, the Keilberg Member, directly overlies the apex of the diamictite buildup. The Rasthof Formation is absent in these sections, implying erosional truncation during the Marinoan glaciation. Before the present study (Hoffman et al. 2016a), the polymictic diamictite of the south dome was erroneously assigned to the Ghaub Formation on account of the (assumed depositional) superposition of the Keilberg Member (Maloof, 2000; Schreiber, 2006; Hoffman and Halverson, 2008). The anomalous basement-derived composition of the diamictite was acknowledged. The Ghaub Formation diamictites are generally derived almost exclusively from the upper Abenab Subgroup (Domack and Hoffman, 2011; Hoffman, 2011), because the Marinoan glaciation occurred after the rift-to-shelf transition (Fig. 2). In contrast, the Sturtian glaciation occurred during a period of crustal stretching, exposing the entire Ugab Subgroup and crystalline basement to glacial erosion on rift shoulders. Before the present study, the occurrence of the 2.4-m-thick Rasthof Formation on the flanks of the buildup (columns B–D and H–K, Figs. 13, 14, 16) was missed.

How did the 223-m-high wedge of diamictite originate? It is not a paleoesker because it is not composed of sand. A kame is similarly unlikely because well-sorted facies (e.g., conglomerate and siltstone) are minor (Fig. 16).

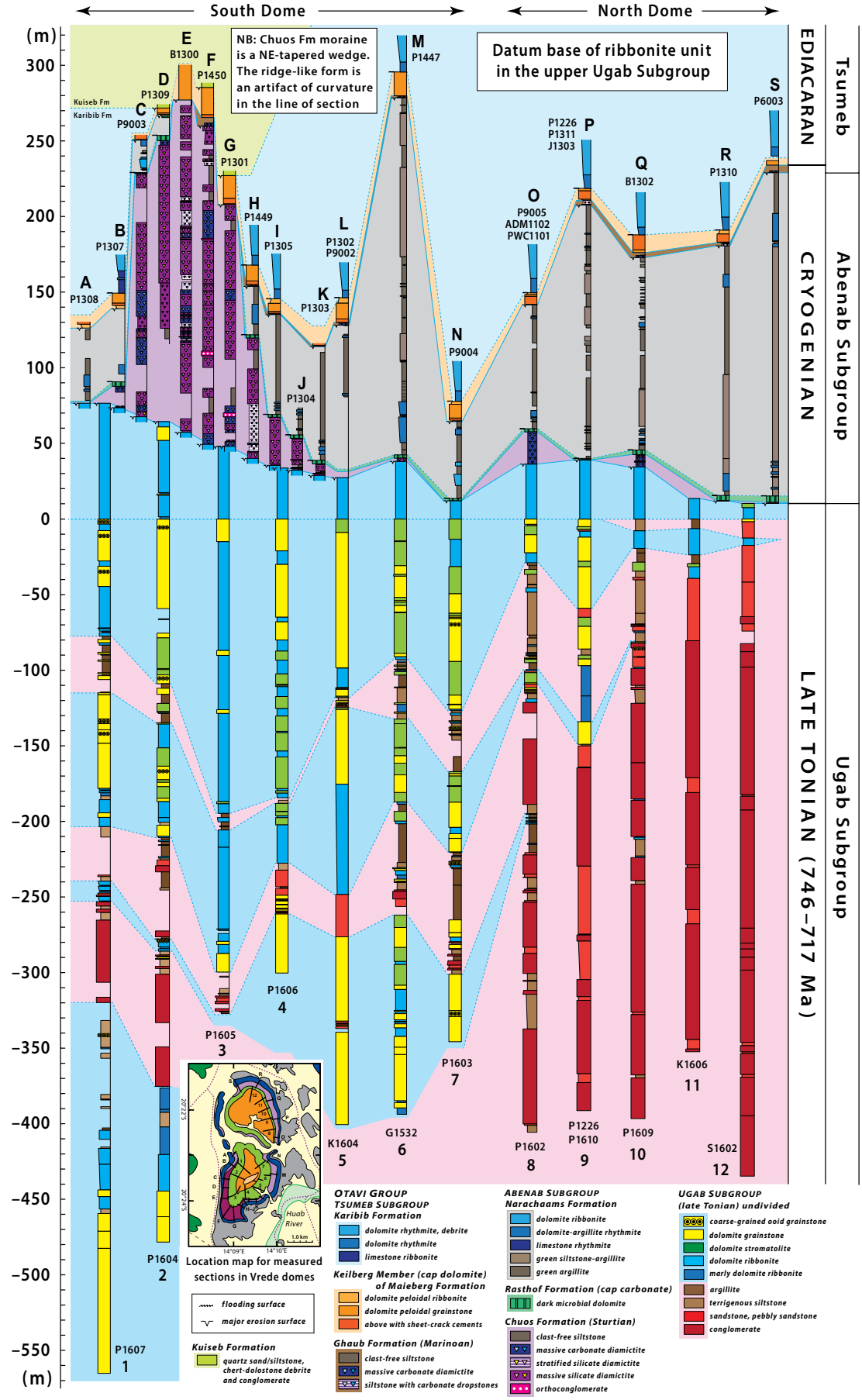

Figure 15. Columnar sections of the Ugab, Abenab, and lower Tsumeb Subgroups, ordered anticlockwise around the Vrede domes (see Fig. 10 for locations). Vertical datum (0 m) is the flooding surface beneath the upper Ugab Subgroup ribbonite unit (Fig. 12). The Chuos Formation diamictite wedge stands with positive relief, like a moraine or erosional outlier, on the Sturtian glacial erosion surface at the top of the Ugab Subgroup (Fig. 16). Draping of the Keilberg Member of Maieberg Formation over the Chuos diamictite wedge is largely a consequence of differential compaction of the argillaceous Narachaams Formation relative to the diamictite. Sharp differences in Narachaams Formation thickness away from the diamictite wedge may reflect differential tectonic strain (e.g., inflating column M at the expense of columns N and O). Using the upper Ugab Subgroup datum for reconstructing the diamictite wedge rather than the Keilberg Member datum (Fig. 13) nullifies differential compaction and strain of the Narachaams Formation. Field number for each section is shown near the column number. NB—nota bene ("notice this well").

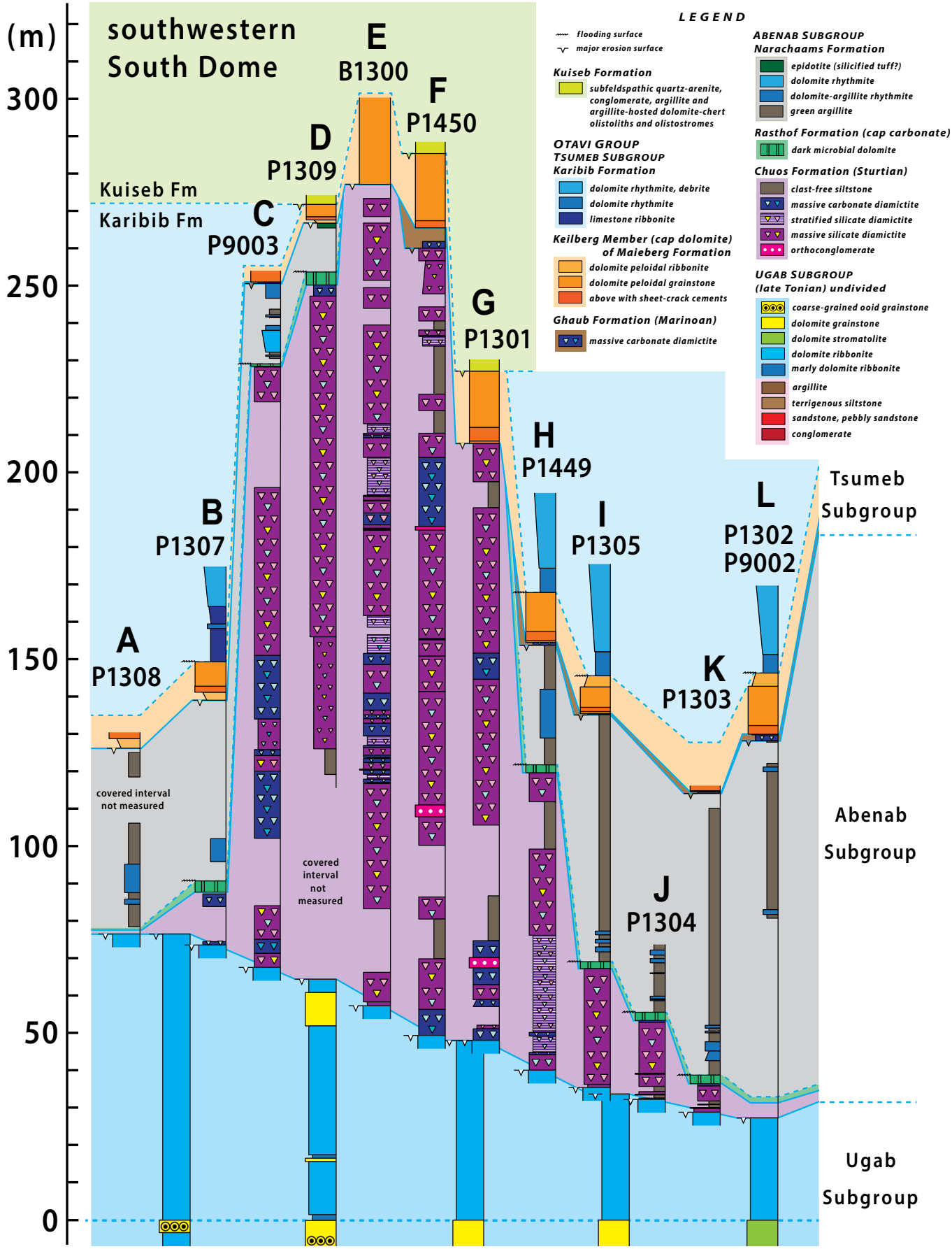

Figure 16. Columnar sections of the Chuos Formation diamictite wedge in the southwestern half of the Vrede south dome (Fig. 10), showing its relations to the Ugab Subgroup, to the Rasthof and Narachaams Formations of the nonglacial Abenab Subgroup (Cryogenian), to the Marinoan glacial erosion surface at the base of the Tsumeb Subgroup, and to the erosional disconformity at the base of the syn-orogenic Kuiseb Formation (Mulden Group). Draping of the Tsumeb Subgroup over the Chuos wedge reflects differential compaction of the argillaceous Narachaams Formation. Decompaction would yield a flatter Marinoan glacial surface beneath the Tsumeb Subgroup. Vertical datum is the same as Figure 15. The apparent bilateral symmetry of the Chuos wedge is an artifact of the curved line of columns (Fig. 10). Field number for each section is shown near the column number.

It could be a composite terminal moraine, but if the expected glacitectonic structures are present (Benn and Evans, 1998), we missed them. A crude horizontal layering (Figs. 14, 16) suggests that the wedge might belong to an erosional outlier composed of previously more continuous sheets of diamictite (ground moraine). But the height of the wedge is four times larger than that of any typical drumlin. From the standpoint of glacial sedimentology, the root frustration is the same as in the previous case study. Because of folding, we have cross-sections a Quaternary geologist would envy, but we know little about the local depositional planform.

CASE 3. SUBGLACIAL HALF GRABEN WITH GROWTH STRATA ON TOEKOMS FARM

The Otavi Group on Toekoms farm is autochthonous with respect to the basement of the Kamanjab inlier (Figs. 3, 17). A thick sequence of coarse- to fine-grained clastic rocks unconformably overlies the basement and dips 46° on average (n = 46) toward the southeast. The clastic sequence is ferruginous toward the top, where it is sharply but conformably overlain by ~230 m of dark-gray limestone, quartz arenite, and limestone turbidites, and redeposited(?) quartz-pebble conglomerate. The limestone unit is continuous with the lower Abenab Subgroup to the west on Bethanis farm (Fig. 17), but the limestone thins abruptly westward across the NNW-striking Soutput growth fault.

Frets (1969) and Schreiber (2006) did not recognize a glacial-periglacial origin for the clastic sequence beneath the limestone unit on Toekoms farm, while Hoffman and Halverson (2008) identified glacigenic diamictite but only at the top of the clastic sequence. As the Marinoan glacigenic diamictite (Ghaub Formation) with its distinctive cap dolomite is emphatically developed higher in the succession (Fig. 18), the older diamictite at the top of the clastic sequence and the overlying limestone unit were consigned to the Sturtian Chuos and Rasthof Formations, respectively, while the bulk of the clastic sequence was correlated with the lower Naauwpoort Formation (Hoffman and Halverson, 2008). The correlations imply a significant disconformity, as upper Naauwpoort Formations volcanism is dated at 747 ± 2 and 746 ± 2 Ma (Hoffman et al., 1996), while the onset of low-latitude Sturtian glaciation is younger than ca. 720 Ma (Macdonald et al., 2010; Rooney et al., 2015).

McGee et al. (2012) first identified diamictite and ice-rafted debris of extrabasinal (basement) origin throughout most of the clastic sequence. Accordingly, they placed the Naauwpoort-Chuos Formation contact much lower in the clastic sequence than previous authors, retaining only the basal breccia and conglomerate in the Naauwpoort Formation (McGee et al., 2012). The present study confirms the main findings of McGee et al. (2012) regarding a syn-glacial age for the bulk of the clastic sequence. While we document an offlap relationship between the basal conglomerate (unit 1, Fig. 19) and the disconformably overlying diamictite-bearing unit, we see no evidence for a major hiatus between them. Evidence for glacial action is absent in unit 1, however, so the possibility remains that the boundary between units 1 and 2 marks the onset of the Sturtian glaciation. If there is no major hiatus, unit 1 should be broadly correlative with the Ugab Subgroup (Figs. 2, 15), rather than with the older Naauwpoort Formation.

Geometry of the Toekoms Mini-Basin

From northeast to southwest, the Chuos Formation thickens from ~800 m to >2000 m in a distance of 5 km (Fig. 19). Thickening is accomplished by the expansion of stratal units and the addition of older offlapping strata. The formation is thickest where it terminates (between sections J and L, Fig. 19) against a northwest-southeast–striking fault that borders a narrow antiform of crystalline basement rock. The overall trend of the fault trace is at a high angle to strike of the Chuos Formation (Fig. 19), but its sinuosity suggests that the dip of the fault plane is shallow. Assuming a shallow dip to the northeast, restoring the Chuos Formation stratification to the horizontal rotates the dip of the fault plane to a north or north-northwest direction (Fig. 2). Northeast of the basement antiform, the Chuos Formation is a fault-bounded and distally tapered wedge, exposed in oblique section (Fig. 19). On the southwest side of the basement antiform, the unconformably overlying Chuos Formation is thin (<140 m; column G, Fig. 18) or absent (column J).

Sedimentology of the Basin Fill

In spite of (weak) tectonic cleavage and widespread fracture-associated ferruginization, sedimentological study of the basin fill is facilitated by lithological diversity, excellent preservation of primary features, and semi-continuous outcrop (Fig. 20A). Our detailed columnar sections (Fig. 19) illustrate a striking juxtaposition of very coarse-grained and very fine-grained deposits, and their strongly asymmetric distribution across the basin. Grain size increases in the direction of stratigraphic thickening, and stratigraphically downward in the more proximal sections (Fig. 19). The fine-grained deposits are strictly subaqueous and are devoid of sedimentary structures generated by wave action or traction currents.

The predominant lithology in more distal sections and in the upper parts of semi-proximal ones is parallel-laminated siltstone-argillite rhythmite (Fig. 20B). Pale yellowish gray in outcrop, the silt-size component takes the form of centimeter-scale graded layers. Subrounded cobbles and boulders of basement granitoid and quartzite occur widely but very sparingly as ice-rafted dropstones (Fig. 20C). Their occurrence is indicated by symbols next to each columnar section in Figure 19. The siltstone-argillite rhythmite is host to decimeter-scale turbidites of coarse silt- to sand-sized detritus (Fig. 20D), and we distinguish these in the columnar sections where they exceed 0.2 m in thickness, either as individual or amalgamated flow units. Climbing ripples occur sparingly in the turbidites, and limited paleocurrent data indicate highly dispersed but modally eastward-directed flows. Turbidites composed of detrital dolomite constitute a minor but locally conspicuous sedimentary component.

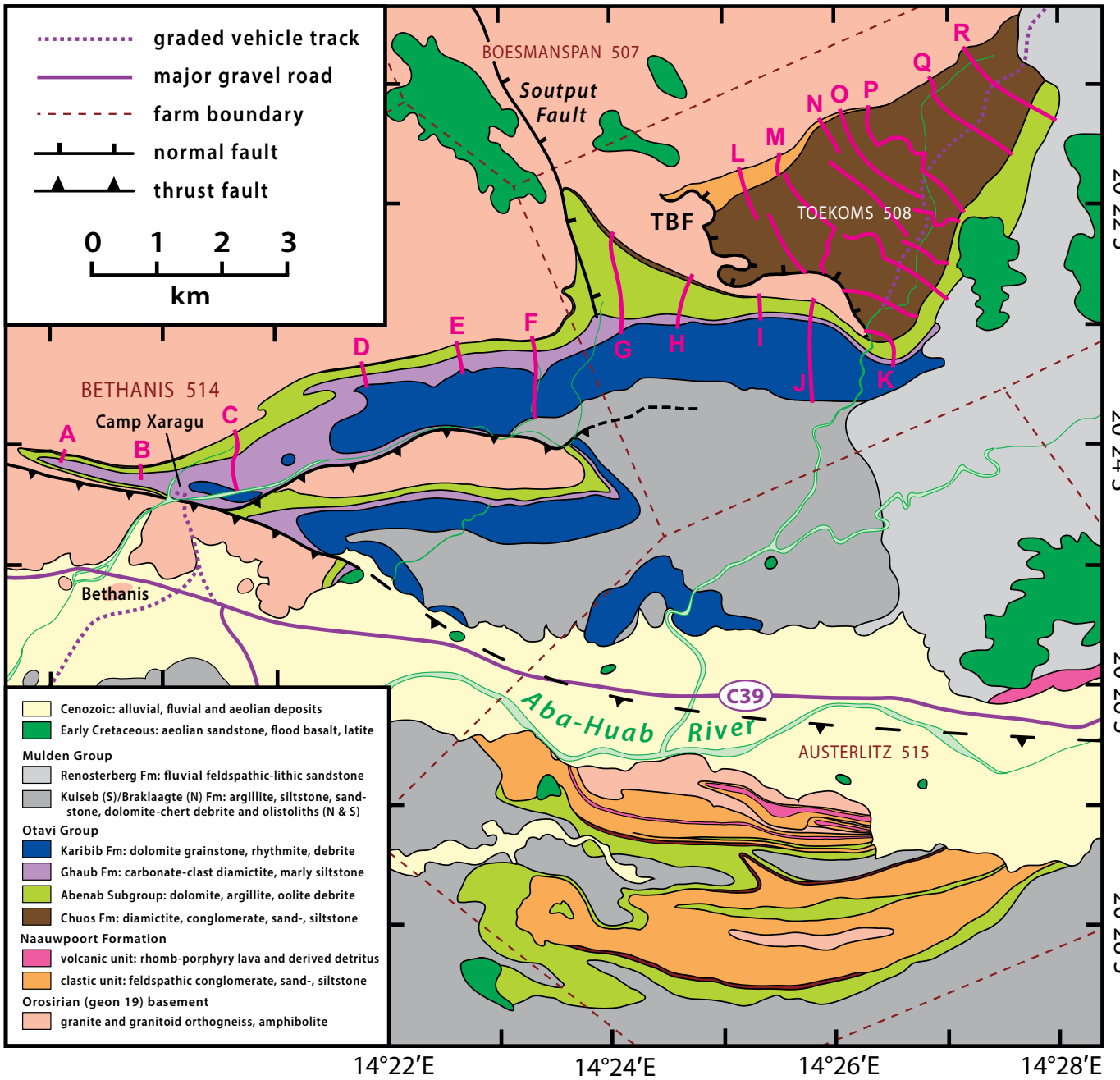

Figure 17. Geology of parts of Bethanis, Austerlitz, and Toekoms farms, Khorixas District, southern Kunene Region, Namibia, showing locations of measured columnar sections (Figs. 18, 19) on the autochthon of the Kamanjab inlier (Fig. 3). Thick-skinned thrusting is associated with the Ediacaran Damara belt collisions. Soutput fault and Toekoms border fault (TBF) are asynchronous Cryogenian growth faults, steeply and gently dipping respectively. Major erosional disconformities occur beneath the allochthonous Kuiseb Formation and the autochthonous-parautochthonous Braklaagte and Renosterberg Formations of the syn-orogenic Mulden Group. The Tsumeb Subgroup (Ghaub and Karibib Formations) is missing in the allochthonous anticlinorium on Austerlitz farm, south of the Aba-Huab River, due to sub-Kuiseb erosion and/or submarine landsliding (Clifford, 2008; Hoffman et al., 2016b). A geon (Hofmann, 1990) equals 100 m.y. and geon 19 is 1900–1999 Ma. Each farm property is identified by name and number.

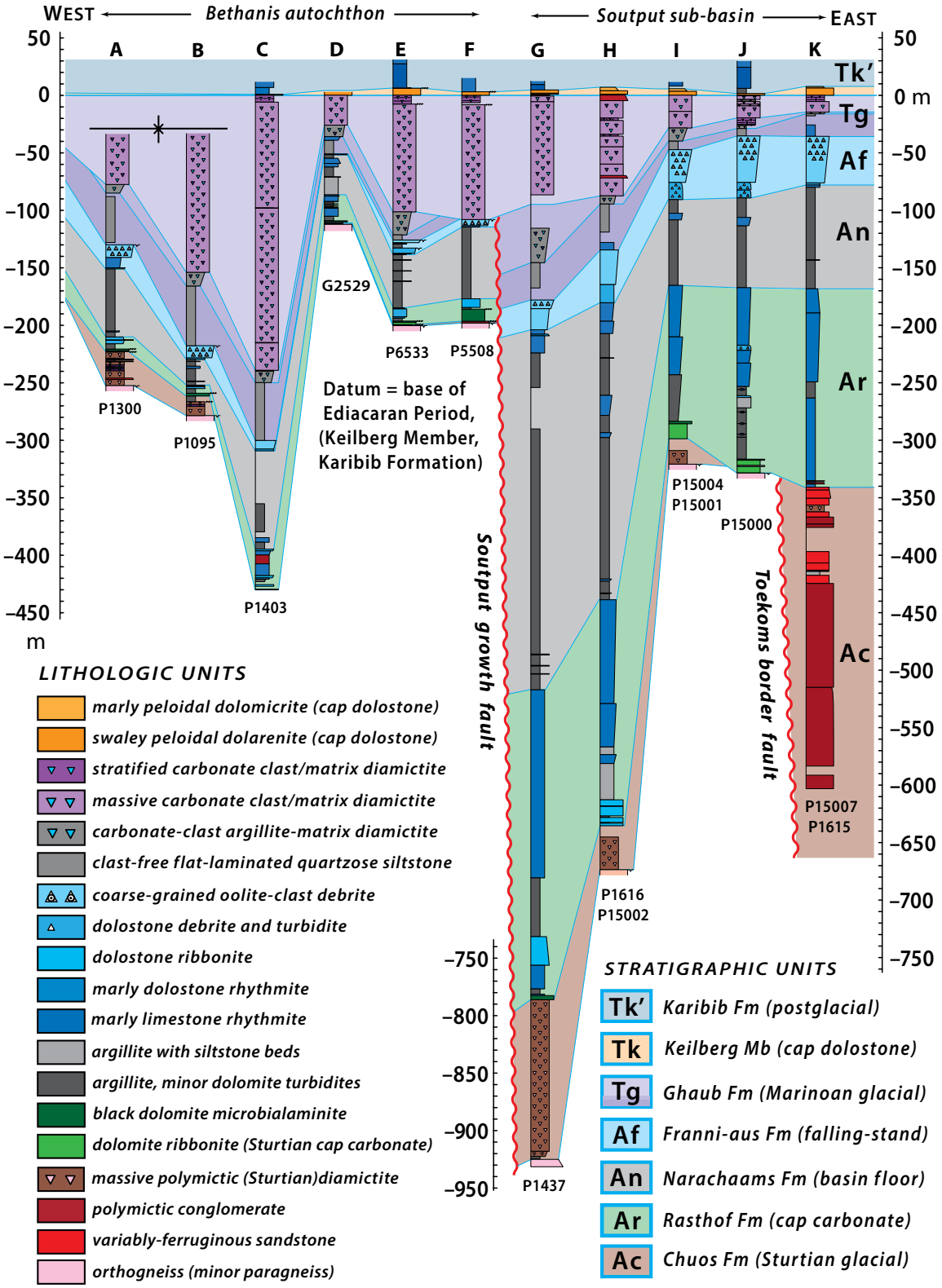

Figure 18. Autochthonous columnar sections of the Abenab and basal Tsumeb Subgroups on Bethanis farm and across the asynchronous Soutput growth fault and Toekoms border fault (see Fig. 17 for locations). Vertical datum (0 m) is the base of the Keilberg Member (Karibib Formation, Tsumeb Subgroup), also the base of the Ediacaran Period. Soutput fault slip ended by middle Ghaub Formation time, and Toekoms by Rasthof Formation time. Soutput fault was not structurally inverted, likely because its strike nearly parallels the direction of Damaran shortening. Note localized thickening of the Marinoan Ghaub Formation on Bethanis farm. Lack of incision suggests that Ghaub thickening represents a positive topographic feature, unrelated to the Soutput growth fault. Field number for each section is shown beneath each column.

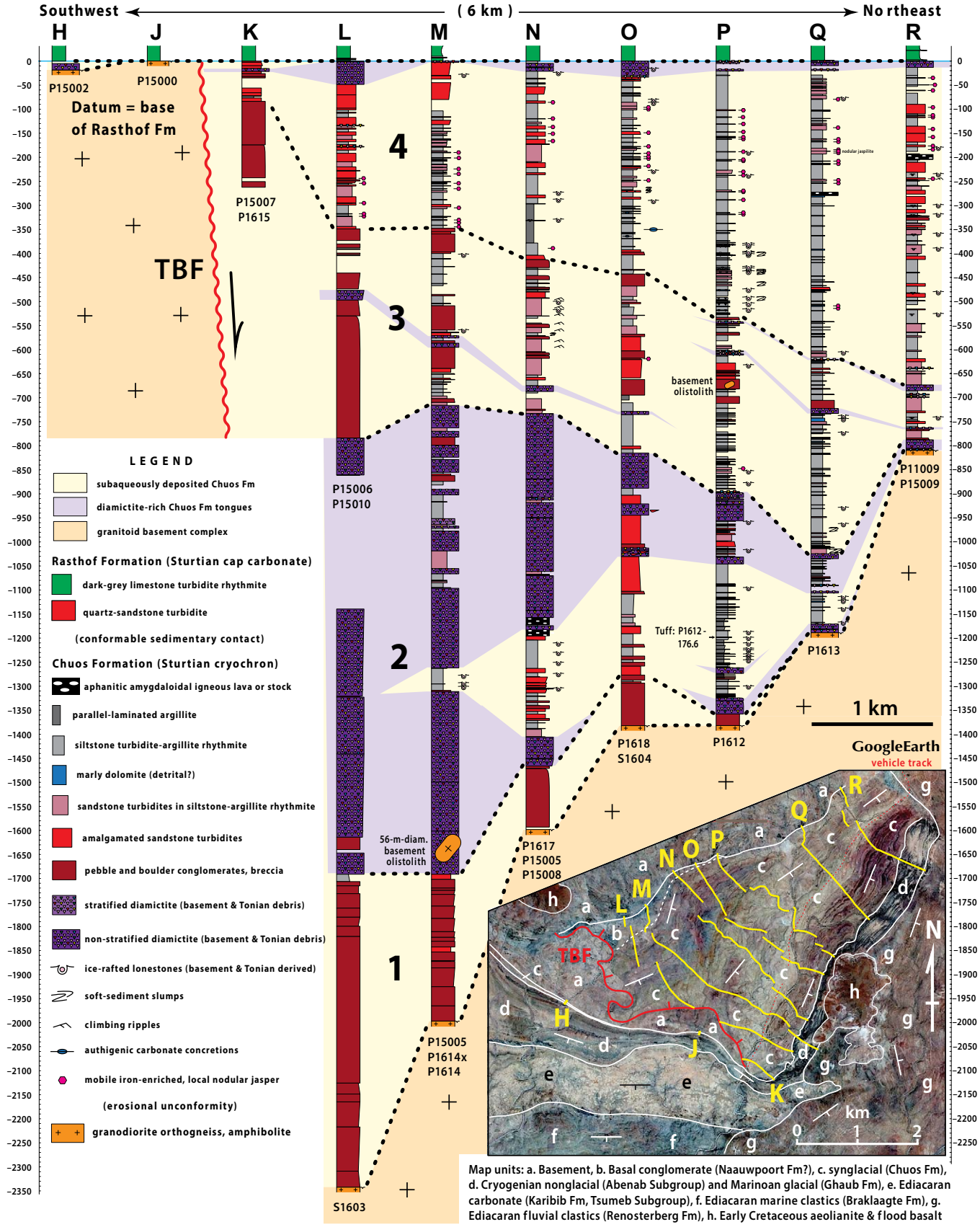

Map units: a. Basement, b. Basal conglomerate (Naauwpoort Fm?), c. synglacial (Chuos Fm), d. Cryogenian nonglacial (Abenab Subgroup) and Marinoan glacial (Ghaub Fm), e. Ediacaran carbonate (Karibib Fm, Tsumeb Subgroup), f. Ediacaran marine clastics (Braklaagte Fm), g. Ediacaran fluvial clastics (Renosterberg Fm), h. Early Cretaceous aeolianite & flood basalt

Figure 19. Columnar sections of the lower Naauwpoort(?) and Chuos Formations in the Toekoms syn-glacial half graben (see Fig. 17 and satellite view inset for locations). Vertical datum (0 m) is the base of the Rasthof Formation cap limestone. Note the thin glacigenic diamictite directly beneath the cap limestone in sections K–R inclusive. TBF is the Toekoms border fault, an inferred normal-sense growth-fault detachment. Heavy dotted lines divide the mini-basin into four approximately isochronous units: (1) basal conglomerate unit, (2) main diamictite-bearing unit, (3) siltstone with coarse-grained clastics, and (4) siltstone with turbidites, ferruginized (red dots) distally from the TBF, and dropstones (see satellite inset). Note the shift in the locus of maximum accumulation from TBF proximal to TBF distal over time (Fig. 21). Field number for each section is shown beneath each column. See Figure 17 for inset coordinates.

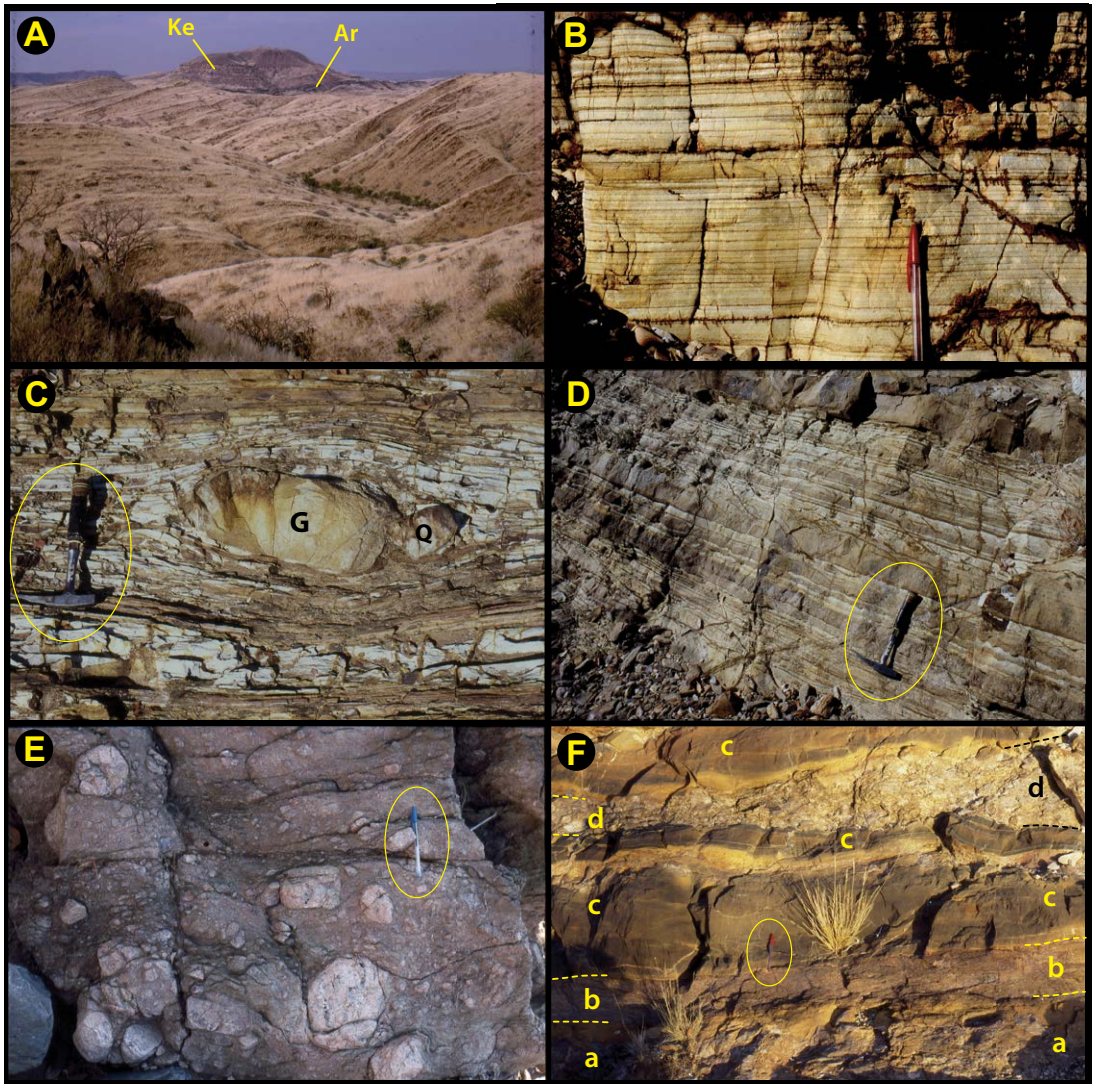

Figure 20. Field images from the syn-glacial half graben on Toekoms farm. (A) View looking southward across the basin from the base of columnar section R (Fig. 19). The prominent hill, 3 km distant, center is an Early Cretaceous flood-basalt outlier (unit Ke), at the base of which the thin black band is the Rasthof Formation (unit Ar) cap limestone. (B) Parallel-laminated silty argillite in the upper part of columnar section N. (C) Ice-rafted dropstones of granodiorite (G) and quartz-arenite (Q) in parallel-laminated silty argillite from the upper part of columnar section N. (D) Graded turbidite beds of quartz arenite in silty argillite in the middle part of columnar section P. (E) Sandy conglomerate from the basal part of columnar section M. (F) Sharp conformable base of the Rasthof Formation cap limestone (unit c) at the top of columnar section Q. Lithologic units: a—basement-clast diamictite with detrital dolomite matrix; b—basement-derived feldspathic greywacke; c—dark-gray micritic limestone; d—quartz-pebble conglomerate interbed. Stratigraphic conformity is implied by the persistence of a thin basement-clast diamictite beneath the Rasthof Formation in sections K–R inclusive.

In the upper 250–500 m of sections L–R, the turbidites are selectively ferruginized (Fig. 19). Soft-sediment slumps involving single flow units or intervals several meters in thickness are common. Because the larger slumps appear to have lobe-like geometry, we did not attempt to infer transport directions from soft-sediment fold orientations. A single set of soft-sediment thrust imbricates 645 m above the base of section N (Fig. 19) indicates transport directed southwestward (230° azimuth), consistent with tilting of the sediment surface toward the border fault.

There are two classes of coarse-grained deposits, diamictite and conglomerate. The former consists of unsorted mixtures in which a matrix of sand-, silt-, and clay-size detritus holds variably dispersed, subrounded, outsized clasts composed of crystalline basement lithologies and variable proportions of

quartz arenite and dolomite. As the latter are absent in the pre-Sturtian paleogeology of the immediate area, it is tempting to infer glacial transport from south to north, as the Ugab Subgroup in the northernmost Damara belt allochthon (e.g., Vrede domes) is and was the closest source of Tonian sedimentary rocks. The diamictite bodies are overwhelmingly massive to weakly stratified, and the latter are commonly disturbed. They thicken and amalgamate toward the southwest border fault, forming composite diamictite intervals up to 470 m thick (column L, Fig. 19). Directly adjacent to the fault, diamictite is interlayered with conglomerate, but more distally (columns M–R, Fig. 19) the diamictite bodies are bounded by siltstone-argillite rhythmite and associated turbidites. It is possible that many of the diamictite bodies are resedimented. Fabric analysis was not attempted because of the generally equant shapes of the clasts. Enclosed within the lowest diamictite unit in columnar section M (Fig. 19) is a 56-m-long olistolith of granodiorite orthogneiss and pegmatitic granite, exposed in a drainage at 20°21.970′S, 14°29.391′E. The occurrence of a relatively thin and stratigraphically isolated diamictite at or close to the top of the Chuos Formation in columns K–R inclusive (Fig. 19) implies that the contact with the overlying Rasthof Formation is conformable.

The conglomerates are bodies of clast-supported boulders or cobbles, mostly well rounded and composed of locally derived granodiorite, pegmatitic granite, vein quartz, and amphibolite in order of declining abundance. At the base of the sedimentary sequence in columnar sections K–P (Fig. 19) is a composite, crudely stratified conglomerate containing meter-scale lenses of moderately well-sorted sandstone and pebbly sandstone. This composite basal conglomerate attains a maximum thickness of 635 m in column L, yet is missing altogether 3–4 km along strike in columns Q and R (Fig. 19). Stratigraphically higher, above the main diamictite bodies, is a cluster of discrete conglomerate units hosted within sandstone turbidites and siltstone-argillite rhythmite (Fig. 19). These sharp-based conglomerates may have been gravitationally redeposited given the lack of traction-current deposits in the enveloping strata.

Origin of the Basin

The geometry of the basin, including the stratal geometry of its sedimentary fill, leaves little room for doubt that it was an active half graben. The stratal geometry is directly comparable to that of growth strata in Mesozoic rift basins of the proto–North Atlantic imaged in seismic reflection data (e.g., Fig. 21). The seismic data map impedance contrast, which is lithologically controlled. We do likewise in selecting five surfaces across which there is a major lithologic change (Figs. 19, 21A). They divide the basin fill into four stratigraphic intervals, which given the small size of the basin we assume to be nearly isochronous. The surfaces are the top of the crystalline basement, the top of the basal conglomerate, the top of the main cluster of diamictites, the top of the coarse-grained clastics above the main diamictite, and the base of the Rasthof Formation cap limestone. Stratigraphic intervals 1 and 2 thicken toward the border detachment fault (Figs. 19, 21A). Interval 3 changes little in thickness, and interval 4 thickens away from

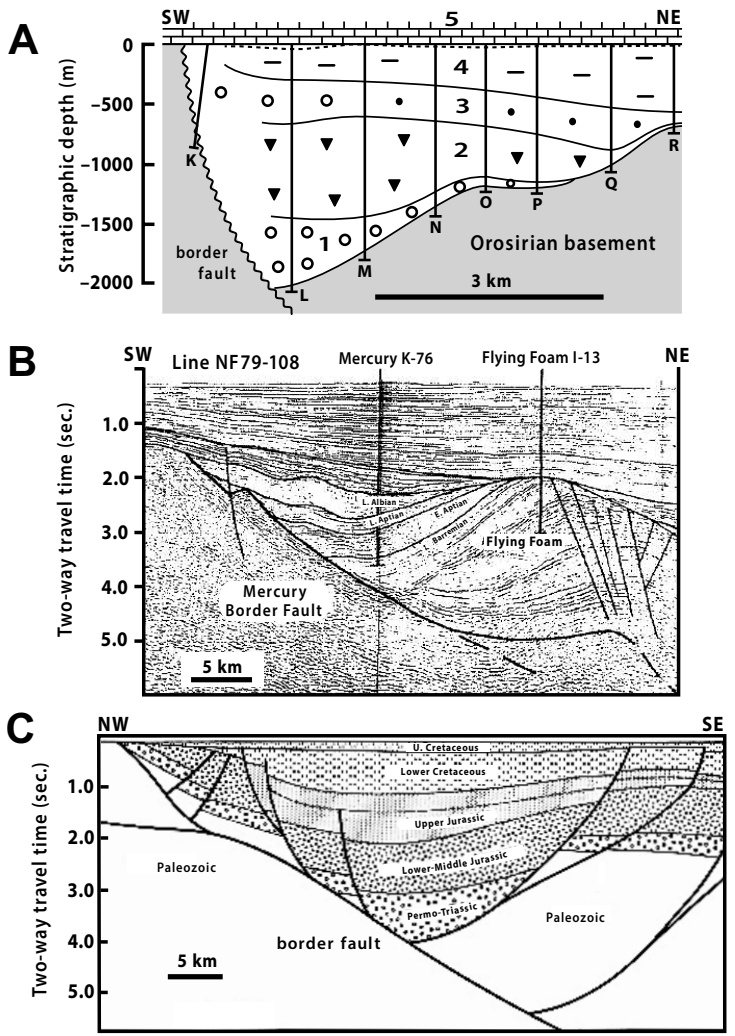

Figure 21. Comparison of syn-rift growth strata in Toekoms half graben (A) with Mesozoic rift basins of the North Atlantic margins imaged in seismic-reflection lines: Jeanne d'Arc Basin, offshore Newfoundland (B) (redrawn from Driscoll et al., 1995) and North Celtic Sea Basin, offshore Ireland (C) (redrawn from Petrie et al., 1989). Inferred time lines in A separate the basal conglomerate complex (1), main diamictite-bearing interval (2), intermittent coarse-grained interval (3), upper fine-grained interval (4), and Rasthof Formation cap limestone (5), as indicated in Figure 19. Dashed line directly below the cap limestone is the base of the terminal diamictite. In all three sections the locus of most rapid sediment accumulation shifted from proximal to distal over time with respect to the border fault. Columns in A are as in Figure 19.

the border fault. The same proximal-to-distal shift in the locus of maximum accumulation is observed in seismically imaged half grabens of Jurassic (Petrie et al., 1989) and Cretaceous (Driscoll et al., 1995) age in the North Atlantic (Figs. 21B, 21C). The comparison suggests that, like the Mesozoic structures, the Toekoms half graben was a hanging-wall basin above a listric, normal-sense detachment (McClay, 1989; Tankard et al., 1989; Driscoll et al., 1995).

The Toekoms growth fault had a north-side-down sense of slip, before it was tilted during collisional orogeny and growth of the Kamanjab inlier as discussed previously. Its kinematics were antithetic to those of contemporaneous growth faults to the north, inferred to be south-side-down from stratigraphic-sedimentologic records of footwall ("rift shoulder") uplift and dip-slope denudation (Hoffman and Halverson, 2008). The Makalani uplift (Fig. 2) was intermittently active for over 100 m.y., from Devede (ca. 760 Ma) through Gruis (ca. 650 Ma) Formation time. Huab uplift was active from Chuos through Gruis Formation time. The stratal geometry of Toekoms basin (Fig. 21) is consistent with a listric master detachment. It is conceivable that rapid differential subsidence responsible for the regional platform-to-basin zonation following the Sturtian glaciation was a consequence of slip on a north-dipping, crustal-scale detachment system, of which Toekoms basin is a surface expression.

How does the Toekoms fault growth compare in age with the Sturtian cryochron? The onset of faulting should correspond to the basal conglomerate at the foot of the border fault. It is not known if the area was glaciated at that time, or if the glacial onset corresponds to the conglomerate-diamictite transition (Fig. 19). We collected a tuff (sample P1612-176.6), 152 m above the top of the conglomerate in column P (Fig. 19), in hopes of constraining the conglomerate-diamictite transition radiometrically. The glacial termination is indicated by the abrupt change in sedimentation between the uppermost diamictite and the Rasthof Formation cap limestone (Fig. 20F). Faulting must have ceased by this time because the basal Rasthof Formation strikes across the fault trace without disturbance (Figs. 17, 18, and inset in Fig. 19). Interestingly, slip on the nearby Soutput growth fault (Figs. 17, 18), which began during the Sturtian glaciation, lasted throughout the inter-cryochron and even into the early Marinoan, based on stratal thickening of the Chuos, Rasthof, Narachaams, Franni-aus, and lower Ghaub Formations across its trace (Fig. 18). The amount of post–Narachaams Formation slip is not large, <140 m assuming a failure angle of 60° for the fault plane.

Did Toekoms half graben develop into a subglacial lake? This is a difficult question to answer. The fine parallel-laminated "background" sedimentation (Fig. 20B) is characteristic of lakes. The total absence, above the basal conglomerate (unit 1, Fig. 21A), of sedimentary structures caused by wave action, traction currents, or subaerial exposure is compatible with a subglacial setting. The stratigraphic regularity and low concentration of ice-rafted dropstones is arguably more consistent with ice-shelf rafting as opposed to iceberg rafting. The sedimentary fill is bimodal in grain size, with a paucity of sand relative to coarser- and finer-grained deposits (Fig. 19). It is unclear how this should be interpreted—as due to an absence of open shorefaces, or to their presence somewhere beyond the area of outcrop.

DISCUSSION

Surprisingly few moraines, paleovalleys, or rift basins of Cryogenian age have been described in the literature. Perhaps this is because few papers describing Cryogenian glacial deposits sedimentologically present data from under- or overlying nonglacial formations.

Reusch (1891) famously described a moraine at least 55 m long and 4 m high, resting upon a glacially striated bedrock pavement in the Varangfjord area of North Norway. Reusch's moraine is interpreted to be a melt-out tillite of Marinoan age in a marine setting (Reading and Walker, 1966; Edwards, 1984; Rice et al., 2012). An extremely tall (602 m) and steep (0.08 aspect ratio) moraine of the same age stands within a broad but shallow (100-m-deep) ice-cut trough on the upper foreslope of the Otavi platform, 60 km to the ENE of Toekoms half graben (Hoffman, 2005, 2011; Domack and Hoffman, 2011). This double-crested, bilateral structure could be a medial moraine, marking a stable confluence of tributary glaciers within a trunk ice stream.

A narrow paleochannel (65 m wide by 120 m deep) of Sturtian age (Areyonga Formation) is incised into Tonian carbonate (Bitter Springs Formation) at Ellery Creek in the Amadeus Basin of central Australia (Lindsay, 1989). In South Australia, Dyson and von der Borch (1994) mapped one side of a 150-m-deep paleovalley filled by sandstone that formed toward the end of Marinoan glaciation, after ice-sheet withdrawal but before cap-dolomite sedimentation. In the same region, an erosion surface with nearly 200 m of relief underlies the Marinoan syn-glacial Elatina Formation, based on C-isotope stratigraphy of subglacial strata (Rose et al., 2013). Sturtian bedrock troughs up to 210 m deep are incised into crystalline basement rocks and filled by a progradational stack of stratified glaciomarine diamictites, beautifully exposed, on the Mirbat coast of southern Oman (Kellerhals and Matter, 2003; Rieu et al., 2006). A pair of glacially eroded paleovalleys filled by diamictite and greywacke of the Cryogenian Mineral Fork Formation are described in a field excursion guide to the Big and Little Cottonwood Canyon area near Salt Lake City, Utah, USA (Christie-Blick, 1997). The paleovalleys are incised into late Tonian(?) quartz arenite and siltstone (Big Cottonwood Formation) and are estimated to be 0.9 km deep by 7 km wide and 425 m deep by 2 km wide, respectively.

Sedimentological evidence for subglacial meltwater in a bedrock trough like the one at Omutirapo springs suggests that the trough was occupied by an ice stream, even if it is uncertain whether the trough was excavated by the ice stream or by an ancestral valley glacier (Bentley, 1987; Bamber et al., 2000; Bennett, 2003; Ottesen et al., 2005; Kessler et al., 2008). Ice streams develop in a coupled ice sheet–atmosphere general circulation model (Laboratoire de Glaciologie et de Géophysique de l'Environnement ice sheet model–Laboratoire de Météorologique Dynamique atmosphere general circulation model) prescribed with an ice-covered ocean (Donnadieu et al., 2003). This is not surprising because low accumulation rates of meteoric ice in a Snowball Earth (Abbot et al., 2013) result in relatively old and consequently warm basal ice, facilitating ice-stream development despite little frictional heat production within the generally slow-moving ice sheet (Rignot and Mouginot, 2012). There

are many more subglacial lakes in East Antarctica than in Greenland, where the ice accumulates ~20× faster.

Many authors have invoked rift faulting as a basin-forming mechanism during Cryogenian glaciation (e.g., Eisbacher, 1985; Young and Gostin, 1991; Link et al., 1994; Prave, 1999; Leather et al., 2002; Eyles and Januszczak, 2004; Allen et al., 2004). Yet with few exceptions (e.g., Young and Gostin, 1989), the case for rift faulting was based on sedimentary facies models, not on observed faults with documented growth strata or stratigraphically constrained displacement histories.

CONCLUSIONS

Our investigation of three localized thickenings of the syn-glacial Chuos Formation of Sturtian age (717–659 Ma) was critically informed by closely spaced (<1.0 km) measured sections of the under- and overlying (nonglacial) formations, which allow us to discriminate incised paleovalley deposits from moraine-like buildups.

The first case study (Omutirapo springs) revealed a steep-sided bedrock trough incised into Tonian peritidal carbonate and clastic strata. The 450-m-deep, 3- to 4-km-wide trough coincides with a high-angle growth fault in the underlying strata that was no longer active during the glacial epoch. Before the Sturtian cap carbonate was deposited, the trough was 10% overfilled by glacial and associated facies, including massive and sheared diamictite, stratified siltstone with ice-rafted debris, and sorted sandstone and conglomerate in decreasing order of abundance. We infer that the bedrock trough was occupied by an ice stream lubricated by transient meltwater cavities.

The second case study (Vrede domes) revealed a steep wedge of glacial deposits where no incision of underlying strata occurred. The 2-km-wide by 223-m-high wedge of massive and stratified diamictite, intercalated with siltstone and minor conglomerate, was draped by a thin Sturtian cap carbonate, onlapped by deep basinal deposits, and erosionally decapitated during the subsequent Marinoan glaciation. We infer that the wedge was either a composite terminal moraine or part of an erosional outlier of a formerly more extensive complex of ground moraines.

In the third case study (Toekoms farm), the thickened Chuos Formation directly overlies crystalline basement rocks. Closely spaced measured sections of the syn-glacial succession reveal a fault-bounded half graben with synkinematic growth strata that thicken to >2000 m adjacent to the border fault. We infer that the border fault was a north-dipping, listric, normal-sense detachment structure. Thick conglomerates that may predate glaciation are followed by resedimented diamictites interfingered distally with turbidites and laminated mudrocks with slumps and ice-rafted lonestones. Faulting had ceased when the Sturtian cap carbonate blanketed the slightly underfilled half graben, which we infer to have developed into a subglacial lake or fjord.

Glaciers both create and destroy small-scale topography. Consequently, glacial deposits are hideously complex in stratigraphic detail. Our approach revealed aspects of Sturtian glacial sedimentation not captured in studies that rely on small numbers of columnar sections spaced tens or hundreds of kilometers apart, or on data from syn-glacial formations in isolation. We do not claim to have thoroughly investigated the glacial sedimentology in our case studies, but we did discover depositional contexts that will make such investigations more meaningful.

If we ignore the climatic implications of the carbonate platform within which the Chuos Formation occurs (Fig. 2), the sedimentary depocenters described here could represent a Quaternary-like regional-scale glaciation. Cryogenian and younger glacial deposits are essentially indistinguishable lithologically (Spencer, 1971; Edwards, 1984; Deynoux, 1985; Eyles, 1993; Crowell, 1999; Eyles and Januszczak, 2004; Étienne et al., 2007; Spence et al., 2016). Only their regional- and time-averaged accumulation rates set Cryogenian glaciations sedimentologically apart from all younger glaciations (Partin and Sadler, 2016).

ACKNOWLEDGMENTS

Most of the data assembled for this study were collected in the austral winters of 2013–2016. The work was authorized by the Geological Survey of Namibia and supported by the Canadian Institute for Advanced Research. PFH is indebted to glacial sedimentologist Marc B. Edwards for the gift of his historic reprint collection. KGL, MSWH, and GPH were supported by the National Science and Engineering Research Council of Canada. SJCL and EBH were supported by Harvard University. Carol Dehler, Peter Sadler, and an anonymous reviewer are thanked for suggesting many improvements in the presentation.

REFERENCES CITED

Abbot, D.S., Voigt, A., and Koll, D., 2011, The Jormungand global climate state and implications for Neoproterozoic glaciations: Journal of Geophysical Research, v. 116, D18103, doi:10.1029/2011JD015927.

Abbot, D.S., Voigt, A., Li, D., Le Hir, G., Pierrehumbert, R.T., Branson, M., Pollard, D., and Koll, D.D.B., 2013, Robust elements of Snowball Earth atmospheric circulation and oases for life: Journal of Geophysical Research: Atmospheres, v, 118, p. 6017–6027, doi:10.1002/jgrd.50540.

Allen, P.A., Leather, J., and Brasier, M.D., 2004, The Neoproterozoic Fiq glaciation and its aftermath, Huqf Supergroup of Oman: Basin Research, v. 16, p. 507–534, doi:10.1111/j.1365-2117.2004.00249.x.

Bamber, J.L., Vaughan, D.G., and Joughin, I., 2000, Widespread complex flow in the interior of the Antarctic Ice Sheet: Science, v. 287, p. 1248–1250, doi:10.1126/science.287.5456.1248.

Benn, D.I., and Evans, D.J.A., 1998, Glaciers and Glaciation: London, Arnold, 734 p.

Bennett, M.R., 2003, Ice streams as the arteries of an ice sheet: Their mechanics, stability and significance: Earth-Science Reviews, v. 61, p. 309–339, doi:10.1016/S0012-8252(02)00130-7.

Bentley, C.R., 1987, Antarctic ice streams: A review: Journal of Geophysical Research, v. 92, p. 8843–8858, doi:10.1029/JB092iB09p08843.

Bold, U., Smith, E.F., Rooney, A.D., Bowring, S.A., Buchwaldt, R., Dudás, F.Ő., Ramezani, J., Crowley, J.L., Schrag, D.P., and Macdonald, F.A., 2016, Neoproterozoic stratigraphy of the Zavkhan terrane of Mongolia: The backbone for Cryogenian and early Ediacaran chemostratigraphic records: American Journal of Science, v. 316, p. 1–63, doi:10.2475/01.2016.01.

Buechi, M.W., Frank, S.M., Graf, H.R., Menzies, J., and Anselmetti, F.S., 2017, Subglacial emplacement of tills and meltwater deposits at the base of overdeepened bedrock troughs: Sedimentology, v. 64, p. 658–685, doi:10.1111/sed.12319.

Christie-Blick, N., 1997, Neoproterozoic sedimentation and tectonics in west-central Utah: Brigham Young University Geology Studies, v. 42, Part 1, p. 1–30.

Clifford, T.N., 2008, The geology of the Neoproterozoic Swakob-Otavi transition zone in the Outjo District, northern Damara Orogen, Namibia: South African Journal of Geology, v. 111, p. 117–140, 3 maps, doi:10.2113/gssajg.111.1.117.

Cook, S.J., and Swift, D.A., 2012, Subglacial basins: Their origin and importance in glacial systems and landscapes: Earth-Science Reviews, v. 115, p. 332–372, doi:10.1016/j.earscirev.2012.09.009.

Coward, M.P., 1981, The junction between Pan African mobile belts in Namibia: Its structural history: Tectonophysics, v. 76, p. 59–73, doi:10.1016/0040-1951(81)90253-5.

Crowell, J.C., 1999, Pre-Mesozoic Ice Ages: Their Bearing on Understanding the Climate System: Geological Society of America Memoir 192, 106 p.

Dalton, L., Bosak, T., Macdonald, F.A., Lahr, D.G., and Pruss, S.B., 2013, Preservational and morphological variability of assemblages of agglutinated eukaryotes in cap carbonates of the Rasthof Formation, northern Namibia: Palaios, v. 28, p. 67–79, doi:10.2110/palo.2012.p12-084r.

Deynoux, M., 1985, Terrestrial or waterlain glacial diamictites? Three case studies from the late Proterozoic and late Ordovician glacial drifts in West Africa: Palaeogeography, Palaeoclimatology, Palaeoecology, v. 51, p. 97–141, doi:10.1016/0031-0182(85)90082-3.

Domack, E.W., and Hoffman, P.F., 2011, An ice grounding-line wedge from the Ghaub glaciation (635 Ma) on the distal foreslope of the Otavi carbonate platform, Namibia, and its bearing on the snowball Earth hypothesis: Geological Society of America Bulletin, v. 123, p. 1448–1477, doi:10.1130/B30217.1.

Donnadieu, Y., Fluteau, F., Ramstein, G., Ritz, C., and Besse, J., 2003, Is there a conflict between the Neoproterozoic glacial deposits and the snowball Earth interpretation: An improved understanding with numerical modeling: Earth and Planetary Science Letters, v. 208, p. 101–112, doi:10.1016/S0012-821X(02)01152-4.

Driscoll, N.W., Hogg, J.R., Christie-Blick, N., and Karner, G.D., 1995, Extensional tectonics in the Jeanne d'Arc Basin, offshore Newfoundland: Implications for the timing of breakup between Grand Banks and Iberia, *in* Scrutton, R.A., Stoker, M.S., Shimmield, G.B., and Tudhope, A.W., eds., The Tectonics, Sedimentation and Palaeoceanography of the North Atlantic Region: Geological Society of London Special Publication 90, p. 1–28, doi:10.1144/GSL.SP.1995.090.01.01.

Dyson, I.A., and von der Borch, C.C., 1994, Sequence stratigraphy of an incised-valley fill: The Neoproterozoic Seacliff Sandstone, Adelaide Geosyncline, South Australia, *in* Dalrymple, R.W., Boyd, R., and Zaitlin, B.A., eds., Incised-Valley Systems: Origin and Sedimentary Sequences: SEPM (Society for Sedimentary Geology) Special Publication 51, p. 209–222, doi:10.2110/pec.94.12.0209.

Edwards, M.B., 1984, Sedimentology of the Upper Proterozoic glacial record, Vestertana Group, Finnmark, North Norway: Norges Geologiske Undersøkelse Bulletin, v. 394, p. 1–76.

Eisbacher, G.H., 1985, Late Proterozoic rifting, glacial sedimentation, and sedimentary cycles in the light of Windermere deposition, western Canada: Palaeogeography, Palaeoclimatology, Palaeoecology, v. 51, p. 231–254, doi:10.1016/0031-0182(85)90087-2.

Étienne, J.L., Allen, P.A., Rieu, R., and Le Guerroué, E., 2007, Neoproterozoic glaciated basins: A critical review of the Snowball Earth hypothesis by comparison with Phanerozoic glaciations, *in* Hambrey, M., Christofferson, P., Glasser, N., and Hubbard, B., eds., Glacial Sedimentary Processes and Products: New York, Blackwell, p. 343–399, doi:10.1002/9781444304435.ch19.

Evans, D.A.D., 2003, A fundamental Precambrian–Phanerozoic shift in Earth's glacial style?: Tectonophysics, v. 375, p. 353–385, doi:10.1016/S0040-1951(03)00345-7.

Evans, D.A.D., and Raub, T.D., 2011, Neoproterozoic glacial palaeolatitudes: A global update, *in* Arnaud, E., Halverson G.P., and Shields-Zhou, G., eds., The Geological Record of Neoproterozoic Glaciations: Geological Society of London Memoir 36, p. 93–112, doi:10.1144/M36.7.

Eyles, N., 1993, Earth's glacial record and its tectonic setting: Earth-Science Reviews, v. 35, p. 1–248, doi:10.1016/0012-8252(93)90002-O.

Eyles, N., and Januszczak, N., 2004, 'Zipper-rift': A tectonic model for Neoproterozoic glaciations during the breakup of Rodinia after 750 Ma: Earth-Science Reviews, v. 65, p. 1–73, doi:10.1016/S0012-8252(03)00080-1.

Fabre, S., Berger, G., Chavagnac, V., and Besson, P., 2013, Origin of cap carbonates: An experimental approach: Palaeogeography, Palaeoclimatology, Palaeoecology, v. 392, p. 524–533, doi:10.1016/j.palaeo.2013.10.006.

Frets, D.C., 1969, Geology and structure of the Huab-Welwitschia area, South West Africa: University of Cape Town Precambrian Research Unit Bulletin 5, 235 p. and map.

Gevers, T.W., 1931, An ancient tillite in South-West Africa: Transactions of the Geological Society of South Africa, v. 34, p. 1–17.

Guj, P., 1974, A revision of the Damara stratigraphy along the southern margin of the Kamanjab inlier, South West Africa, *in* Kröner, A., ed., Contributions to the Precambrian Geology of Southern Africa: University of Cape Town Precambrian Research Unit Bulletin 15, p. 167–176.

Halverson, G.P., Hoffman, P.F., Schrag, D.P., Maloof, A.C., and Rice, A.H.N., 2005, Toward a Neoproterozoic composite carbon-isotope record: Geological Society of America Bulletin, v. 117, p. 1181–1207, doi:10.1130/B25630.1.

Hedberg, R.M., 1979, Stratigraphy of the Ovamboland Basin, South West Africa: University of Cape Town Precambrian Research Unit Bulletin 24, 325 p.

Henry, G., Stanistreet, I.G., and Maiden, K.J., 1986, Preliminary results of a sedimentological study of the Chuos Formation in the Central Zone of the Damara Orogen: Evidence for mass flow processes and glacial activity: Communications of the Geological Survey of Namibia, v. 2, p. 75–92.

Higgins, J.A., and Schrag, D.P., 2003, Aftermath of a snowball Earth: Geochemistry Geophysics Geosystems, v. 4, 1028, doi:10.1029/2002GC000403.

Hoffman, P.F., 2005, 28th DeBeers Alex Du Toit Memorial Lecture: On Cryogenian (Neoproterozoic) ice-sheet dynamics and the limitations of the glacial sedimentary record: South African Journal of Geology, v. 108, p. 557–577, doi:10.2113/108.4.557.

Hoffman, P.F., 2011, Strange bedfellows: Glacial diamictite and cap carbonate from the Marinoan (635 Ma) glaciation in Namibia: Sedimentology, v. 58, p. 57–119, doi:10.1111/j.1365-3091.2010.01206.x.

Hoffman, P.F., and Halverson, G.P., 2008, Otavi Group of the western Northern Platform, the Eastern Kaoko Zone and the western Northern Margin Zone, *in* Miller, R.McG., ed., The Geology of Namibia, Volume 2: Neoproterozoic to Lower Palaeozoic: Windhoek, Geological Survey of Namibia, p. 13-69–13-136.

Hoffman, P.F., and Schrag, D.P., 2002, The snowball Earth hypothesis: Testing the limits of global change: Terra Nova, v. 14, p. 129–155, doi:10.1046/j.1365-3121.2002.00408.x.

Hoffman, P.F., Hawkins, D.P., Isachsen, C.E., and Bowring, S.A., 1996, Precise U-Pb zircon ages for early Damaran magmatism in the Summas Mountains and Welwitschia Inlier, northern Damara Belt, Namibia: Communications of the Geological Survey of Namibia, v. 11, p. 47–52.

Hoffman, P.F., Kaufman, A.J., Halverson, G.P., and Schrag, D.P., 1998a, A Neoproterozoic snowball Earth: Science, v. 281, p. 1342–1346, doi:10.1126/science.281.5381.1342.

Hoffman, P.F., Kaufman, J.A., and Halverson, G.P., 1998b, Comings and goings of global glaciations on a Neoproterozoic carbonate platform in Namibia: GSA Today, v. 8, no. 5, p. 1–9.

Hoffman, P.F., Halverson, G.P., Domack, E.W., Husson, J.M., Higgins, J.A., and Schrag, D.P., 2007, Are basal Ediacaran (635 Ma) post-glacial "cap dolostones" diachronous?: Earth and Planetary Science Letters, v. 258, p. 114–131, doi:10.1016/j.epsl.2007.03.032.

Hoffman, P.F., Bellefroid, E.J., Crockford, P.W., de Moor, A., Halverson, G.P., Hodgin, E.B., Hodgskiss, M.S.W., Holtzman, B.K., Jasechko, G.R., Johnson, B.W., and Lamothe, K.G., 2016a, A misfit Cryogenian diamictite in the Vrede domes, Northern Damara Zone, Namibia: Chuos (Sturtian) or Ghaub (Marinoan) Formation? Moraine or paleovalley?: Communications of the Geological Survey of Namibia, v. 17, p. 1–16.

Hoffman, P.F., Bellefroid, E.J., Johnson, B.W., Hodgskiss, M.S.W., Schrag, D.P., and Halverson, G.P., 2016b, Early extensional detachments in a contractional orogen: Coherent, map-scale, submarine slides (mass transport complexes) on the outer slope of an Ediacaran collisional foredeep, eastern Kaoko belt, Namibia: Canadian Journal of Earth Sciences, v. 53, p. 1177–1189, doi:10.1139/cjes-2015-0164.

Hoffmann, K.-H., 1989, New aspects of lithostratigraphic subdivision and correlation of late Proterozoic to early Cambrian rocks of the southern Damara Belt, and their correlation with the central and northern Damara Belt and the Gariep Belt: Communications of the Geological Survey of Namibia, v. 5, p. 59–67.

Hoffmann, K.-H., and Prave, A.R., 1996, A preliminary note on a revised subdivision and regional correlation of the Otavi Group based on glaciogenic diamictites and associated cap dolomites: Communications of the Geological Survey of Namibia, v. 11, p. 81–86.

Hofmann, H.J., 1969, Attributes of stromatolites: Geological Survey of Canada Paper 69-39, 58 p., doi:10.4095/106437.

Hofmann, H.J., 1990, Precambrian time units and nomenclature–the geon concept: Geology, v. 18, p. 340–341, doi:10.1130/0091-7613(1990)018<0340:PTUANT>2.3.CO;2.

Kaufman, A.J., Knoll, A.H., and Narbonne, G.M., 1997, Isotopes, ice ages, and terminal Proterozoic Earth history: Proceedings of the National Academy of Sciences of the United States of America, v. 94, p. 6600–6605, doi:10.1073/pnas.94.13.6600.

Kellerhals, P., and Matter, A., 2003, Facies analysis of a glaciomarine sequence, the Neoproterozoic Mirbat Sandstone Formation, Sultanate of Oman: Eclogae Geologicae Helvetiae, v. 96, p. 49–70.

Kennedy, M.J., Runnegar, B., Prave, A.R., Hoffmann, K.-H., and Arthur, M.A., 1998, Two or four Neoproterozoic glaciations?: Geology, v. 26, p. 1059–1063, doi:10.1130/0091-7613(1998)026<1059:TOFNG>2.3.CO;2.

Kessler, M.A., Anderson, R.S., and Briner, J.P., 2008, Fjord insertion into continental margins driven by topographic steering of ice: Nature Geoscience, v. 1, p. 365–369, doi:10.1038/ngeo201.

Knoll, A.H., Walter, M.R., Narbonne, G.M., and Christie-Blick, N., 2006, The Ediacaran Period: A new addition to the geologic time scale: Lethaia, v. 39, p. 13–30, doi:10.1080/00241160500409223.

Kröner, A., and Rankama, K., 1972, Late Precambrian glaciogenic sedimentary rocks in southern Africa: A compilation with definitions and correlations: University of Cape Town Precambrian Research Unit Bulletin 11, 37 p.

Leather, J.A., Allen, P.A., Brasier, M.D., and Cozzi, A., 2002, Neoproterozoic snowball Earth under scrutiny: Evidence from the Fiq glaciation of Oman: Geology, v. 30, p. 891–894, doi:10.1130/0091-7613(2002)030<0891:NSEUSE>2.0.CO;2.

Le Ber, E., Le Heron, D.P., Winterleitner, G., Bosence, D.W.J., Vining, B.A., and Komona, F., 2013, Microbialite recovery in the aftermath of the Sturtian glaciation: Insights from the Rasthof Formation, Namibia: Sedimentary Geology, v. 294, p. 1–12, doi:10.1016/j.sedgeo.2013.05.003.

Le Ber, E., Le Heron, D.P., and Oxtoby, N.H., 2015, Influence of microbial framework on Cryogenian microbial facies, Rasthof Formation, Namibia, *in* Bosence, D.W.J., Gibbons, K.A., Le Heron, D.P., Morgan, W.A., Prithard, T., and Vining, B.A., eds., Microbial Carbonates in Space and Time: Implications for Global Exploration and Production: Geological Society of London Special Publication 418, p. 111–112, doi:10.1144/SP418.7.

Lechte, M., and Wallace, M., 2016, Sub–ice shelf ironstone deposition during the Neoproterozoic Sturtian glaciation: Geology, v. 44, p. 891–894, doi:10.1130/G38495.1.

Le Heron, D.P., Busfield, M.E., and Kamona, F., 2013a, An interglacial on snowball Earth? Dynamic ice behaviour revealed in the Chuos Formation, Namibia: Sedimentology, v. 60, p. 411–427, doi:10.1111/j.1365-3091.2012.01346.x.

Le Heron, D.P., Busfield, M.E., Le Ber, E., and Kamona, A.F., 2013b, Neoproterozoic ironstones in northern Namibia: Biogenic precipitation and Cryogenian glaciation: Palaeogeography, Palaeoclimatology, Palaeoecology, v. 369, p. 48–57, doi:10.1016/j.palaeo.2012.09.026.

Li, Z.-X., Evans, D.A.D., and Halverson, G.P., 2013, Neoproterozoic glaciations in a revised global palaeogeography from the breakup of Rodinia to the assembly of Gondwanaland: Sedimentary Geology, v. 294, p. 219–232, doi:10.1016/j.sedgeo.2013.05.016.

Lindsay, J.F., 1989, Depositional controls on glacial facies associations in a basinal setting, Late Proterozoic, Amadeus Basin, central Australia: Palaeogeography, Palaeoclimatology, Palaeoecology, v. 73, p. 205–232, doi:10.1016/0031-0182(89)90005-9.

Link, P.K., Miller, J.M.G., and Christie-Blick, N., 1994, Glacial-marine facies in a continental rift environment: Neoproterozoic rocks of the western United States Cordillera, *in* Deynoux, M., Miller, J.M.B., Domack, E.W., Eyles, N., Fairchild, I.J., and Young, G.M., eds., Earth's Glacial Record: Cambridge, UK, Cambridge University Press, p. 29–46, doi:10.1017/CBO9780511628900.003.

Macdonald, F.A., Schmitz, M.D., Crowley, J.L., Roots, C.F., Jones, D.S., Maloof, A.C., Strauss, J.V., Cohen, P.A., Johnston, D.T., and Schrag, D.P., 2010, Calibrating the Cryogenian: Science, v. 327, p. 1241–1243, doi:10.1126/science.1183325.

Maloof, A.C., 2000, Superposed folding at the junction of the inland and coastal belts, Damara Orogen, NW Namibia: Communications of the Geological Survey of Namibia, v. 12, p. 89–98.

Martin, H., 1961, The hypothesis of continental drift in the light of recent advances of geological knowledge in Brazil and in South West Africa: Geological Society of South Africa Alex L. du Toit Memorial Lecture 7, Annexure to Transactions, v. 64, 47 p., 5 plates.

Martin, H., 1964, Beobachtungen zum Problem der jung-präkambrischen Glazialen Ablagerungen in Südwestafrika [Observations concerning the problem of the late Precambrian glacial deposits in South West Africa]: Geologische Rundschau, v. 54, p. 115–127, doi:10.1007/BF01821173.

Martin, H., 1965, The Precambrian Geology of South West Africa and Namaqualand: University of Cape Town Precambrian Research Unit Bulletin 1, 159 p.

Martin, H., 1968, Paläomorphologische Formelemente in den Landschaften Südwest-Afrikas: Geologische Rundschau, v. 58, p. 121–128, doi:10.1007/BF01820598.

Martin, H., Porada, H., and Walliser, O.H., 1985, Mixtite deposits of the Damara sequence, Namibia, problems of interpretation: Palaeogeography, Palaeoclimatology, Palaeoecology, v. 51, p. 159–196, doi:10.1016/0031-0182(85)90084-7.

McClay, K.R., 1989, Physical models of structural styles during extension, *in* Tankard, A.J., and Balkwill, H.R., eds., Extensional Tectonics and Stratigraphy of the North Atlantic Margins: American Association of Petroleum Geologists Memoir 46, p. 95–110.

McGee, B., Halverson, G.P., and Collins, A.S., 2012, Cryogenian rift-related magmatism and sedimentation: South-western Congo Craton, Namibia: Journal of African Earth Sciences, v. 76, p. 34–49, doi:10.1016/j.jafrearsci.2012.09.003.

Miller, R.McG., 1980, Geology of a portion of central Damaraland, South West Africa/Namibia: Geological Survey of South Africa South West Africa Series 6, 78 p., with map and cross-sections in pocket.

Miller, R.McG., 1997, The Owambo Basin of northern Namibia, *in* Selley, R.C. ed., African Basins:: Amsterdam, Elsevier, Sedimentary Basins of the World, v. 3, p. 237–268.

Miller, R.McG., 2008, The Geology of Namibia, Volume 2: Neoproterozoic to Lower Palaeozoic: Windhoek, Geological Survey of Namibia, 515 p.

Miller, R.McG., and Schalk, K.E.L., 1980, Geological map of Namibia: Windhoek, Geological Survey of Namibia, scale 1:1,000,000.

Nascimento, D.B., Ribeiro, A., Trouw, R.A.J., Schmitt, R.S., and Passchier, C.W., 2016, Stratigraphy of the Neoproterozoic Damara Sequence in northwest Namibia: Slope to basin submarine mass transport deposits and olistolith fields: Precambrian Research, v. 278, p. 108–125, doi:10.1016/j.precamres.2016.03.005.

Ottesen, D., Dowdeswell, J.A., and Rise, L., 2005, Submarine landforms and the reconstruction of fast-flowing ice streams within a large Quaternary ice sheet: The 2500-km-long Norwegian-Svalbard margin (57°–80°N): Geological Society of America Bulletin, v. 117, p. 1033–1050, doi:10.1130/B25577.1.

Partin, C.A., and Sadler, P.M., 2016, Slow sediment accumulation sets snowball Earth apart from all younger glacial episodes: Geology, v. 44, p. 1019–1022, doi:10.1130/G38350.1.

Passchier, C., Trouw, R., and da Silva Schmitt, R., 2016, How to make a transverse triple junction: New evidence for the assemblage of Gondwana along the Kaoko-Damara belts, Namibia: Geology, v. 44, p. 843–846, doi:10.1130/G38015.1.

Patton, H., Swift, D.A., Clark, C.D., Livingstone, S.J., and Cook, S.J., 2016, Distribution and characteristics of overdeepenings beneath the Greenland and Antarctic ice sheets: Implications for overdeepening origin and evolution: Quaternary Science Reviews, v. 148, p. 128–145, doi:10.1016/j.quascirev.2016.07.012.

Penck, A., 1905, Glacial features in the surface of the Alps: The Journal of Geology, v. 13, p. 1–19, doi:10.1086/621202.

Petrie, S.H., Brown, J.R., Granger, P.J., and Lovell, J.P.B., 1989, Mesozoic history of the Celtic Sea basins, *in* Tankard, A.J., and Balkwill, H.R., eds., Extensional Tectonics and Stratigraphy of the North Atlantic Margins: American Association of Petroleum Geologists Memoir 46, p. 433–444.

Pierrehumbert, R.T., Abbot, D.S., Voigt, A., and Koll, D., 2011, Climate of the Neoproterozoic: Annual Review of Earth and Planetary Sciences, v. 39, p. 417–460, doi:10.1146/annurev-earth-040809-152447.

Prave, A.R., 1999, Two diamictites, two cap carbonates, two $\delta^{13}C$ excursions, two rifts: The Neoproterozoic Kingston Peak Formation, Death Valley, California: Geology, v. 27, p. 339–342, doi:10.1130/0091-7613(1999)027<0339:TDTCCT>2.3.CO;2.

Prave, A.R., Condon, D.J., Hoffmann, K.-H., Tapster, S., and Fallick, A.E., 2016, Duration and nature of the end-Cryogenian (Marinoan) glaciation: Geology, v. 44, p. 631–634, doi:10.1130/G38089.1.

Pruss, S.B., Bosak, T., Macdonald, F.A., McLane, M., and Hoffman, P.F., 2010, Microbial facies in a Sturtian cap carbonate, the Rasthof Formation, Otavi Group, northern Namibia: Precambrian Research, v. 181, p. 187–198, doi:10.1016/j.precamres.2010.06.006.

Reading, H.G., and Walker, R.G., 1966, Sedimentation of Eocambrian tillites and associated sediments in Finnmark, northern Norway: Palaeogeography, Palaeoclimatology, Palaeoecology, v. 2, p. 177–212, doi:10.1016/0031-0182(66)90016-2.

Reusch, H., 1891, Skuringmærker og morængrus eftervist i Finnmarken fra en periode meget ældre end 'istiden' [Glacial striae and boulder-clay in Norwegian Lapponie from a period much older than the last ice age]: Norges Geologiske Undersøkelse, Årbok 1891, v. 1, p. 78–85 and 97–100.

Rice, A.H.N., Edwards, M.B., and Hansen, T.A., 2012, Neoproterozoic glacial and associated facies in the Tanafjord–Varangerfjord area, Finnmark, North Norway: Geological Society of America Field Guide 26, 83 p., doi:10.1130/2012.0026.

Ridgwell, A.J., Kennedy, M.J., and Caldeira, K., 2003, Carbonate deposition, climate stability, and Neoproterozoic ice ages: Science, v. 302, p. 859–862, doi:10.1126/science.1088342.

Rieu, R., Allen, P.A., Etienne, J.L., Cozzi, A., and Wiechert, U., 2006, A Neoproterozoic glacially influenced basin margin succession and 'atypical' cap carbonate associated with bedrock paleovalleys, Mirbat area, southern Oman: Basin Research, v. 18, p. 471–496, doi:10.1111/j.1365-2117.2006.00304.x.

Rignot, E., and Mouginot, J., 2012, Ice flow in Greenland for the International Polar Year 2008–2009: Geophysical Research Letters, v. 39, L11501, doi:10.1029/2012GL051634.

Rooney, A.D., Macdonald, F.A., Strauss, J.V., Dudás, F.Ö., Hallmann, C., and Selby, D., 2014, Re-Os geochronology and coupled Os-Sr isotope constraints on the Sturtian snowball Earth: Proceedings of the National Academy of Sciences of the United States of America, v. 111, p. 51–56, doi:10.1073/pnas.1317266110.

Rooney, A.D., Strauss, J.V., Brandon, A.D., and Macdonald, F.A., 2015, A Cryogenian chronology: Two long-lasting synchronous Neoproterozoic glaciations: Geology, v. 43, p. 459–462, doi:10.1130/G36511.1.

Rose, B.E.J., 2015, Stable "Waterbelt" climates controlled by tropical ocean heat transport: A non-linear coupled climate mechanism of relevance to Snowball Earth: Journal of Geophysical Research: Atmospheres, v. 120, p. 1404–1423, doi:10.1002/2014JD022659.

Rose, C.V., Maloof, A.C., Schoene, B., Ewing, R.C., Linnemann, U., Hofmann, M., and Cottle, J.M., 2013, The end-Cryogenian glaciation of South Australia: Geoscience Canada, v. 40, p. 256–293, doi:10.12789/geocanj.2013.40.019.

Schreiber, U.M., 2006, Geological map of Namibia, sheet 2014—Fransfontein: Windhoek, Geological Survey of Namibia, scale 1:250,000.

Spence, G.H., Le Heron, D.P., and Fairchild, I.J., 2016, Sedimentological perspectives on climatic, atmospheric and environmental change in the Neoproterozoic Era: Sedimentology, v. 63, p. 253–306, doi:10.1111/sed.12261.

Spencer, A.M., 1971, Late Pre-Cambrian Glaciation in Scotland: Geological Society of London Memoir 6, 99 p.

Stanistreet, I.G., Kukla, P.A., and Henry, G., 1991, Sedimentary basinal responses to a Late Precambrian Wilson Cycle: The Damara Orogen and Nama Foreland, Namibia: Journal of African Earth Sciences, v. 13, p. 141–156, doi:10.1016/0899-5362(91)90048-4.

Tankard, A.J., Welsink, H.J., and Jenkins, W.A.M., 1989, Structural styles and stratigraphy of the Jeanne d'Arc Basin, Grand Banks of Newfoundland, *in* Tankard, A.J., and Balkwill, H.R., eds., Extensional Tectonics and Stratigraphy of the North Atlantic Margins: American Association of Petroleum Geologists Memoir 46, p. 265–282.

Trindade, R.I.F., and Macouin, M., 2007, Palaeolatitude of glacial deposits and palaeogeography of Neoproterozoic ice ages: Comptes Rendus Geoscience, v. 339, p. 200–211, doi:10.1016/j.crte.2007.02.006.

Wallace, M.W., Hood, A.S., Woon, E.M.S., Hoffmann, K.-H., and Reed, C.P., 2014, Enigmatic chambered structures in Cryogenian reefs: The oldest sponge-grade organisms?: Precambrian Research, v. 255, p. 109–123, doi:10.1016/j.precamres.2014.09.020.

Yoshioka, H., Asahara, Y., Tojo, B., and Kawakami, S., 2003, Systematic variations in C, O, and Sr isotopes and elemental concentrations in Neoproterozoic carbonates in Namibia: Implications for a glacial to interglacial transition: Precambrian Research, v. 124, p. 69–85, doi:10.1016/S0301-9268(03)00079-2.

Young, G.M., and Gostin, V.A., 1989, An exceptionally thick upper Proterozoic (Sturtian) glacial succession in the Mount Painter area, South Australia: Geological Society of America Bulletin, v. 101, p. 834–845, doi:10.1130/0016-7606(1989)101<0834:AETUPS>2.3.CO;2.

Young, G.M., and Gostin, V.A., 1991, Late Proterozoic (Sturtian) succession of the North Flinders Basin, South Australia: An example of temperate glaciation in an active rift setting, *in* Anderson, J.B., and Ashley, G.M., eds., Glacial Marine Sedimentation: Paleoclimatic Significance: Geological Society of America Special Paper 261, p. 207–222, doi:10.1130/SPE261-p207.